Master thesis

Towards robust autonomy of underwater vehicles in Arctic operations

---

Jens E. Bremnes

July 12, 2019

Supervisor: Asgeir J. Sørensen

Norwegian University of Science and Technology
Department of Marine Technology

NTNU Trondheim
Norwegian University of Science and Technology
Department of Marine Technology

MASTER THESIS IN MARINE CYBERNETICS

SPRING 2019

FOR

M.SC. STUDENT JENS EINAR BREMNES

Towards robust autonomy of underwater vehicles in Arctic operations

Work description

Autonomous systems are emerging and essential for allowing new and challenging operations, such as mapping and monitoring of oceans and areas on land in harsh conditions, inspections and interventions of structures difficult to access, and autonomous transportation, both land-based and at sea. As the level of autonomy in systems increases, and the missions become more complex, stricter requirements related to safe system performance and robustness are imposed.

The aim of this Master thesis is to investigate tools and methods for developing more robust autonomy solutions for AUVs operating under the sea ice in the Arctic. This work is a continuation of the candidate's previous work. This thesis will consist of a resume and two scientific conference papers. The first paper proposes a method for the design of a sensor-based hybrid translational observer for underwater navigation, accounting for noisy, asynchronous and sporadically available sensor measurements. The second paper will investigate methods for altitude estimation and control for under-ice operations of AUVs, in conjunction with Artificial Intelligence-based methods for online risk-based reasoning and decision-making for autonomous altitude setpoint selection.

Scope of work

Resume:

1. Describe the motivation for using AUVs as sensor platforms for Arctic marine research, and the research challenges related to navigation, autonomy and online risk management
2. Present the case; Arctic operations of AUVs, including details about the missions.
3. Review relevant literature related to guidance, navigation and control of AUVs operating under ice, hybrid dynamical systems, Bayesian risk modelling and decision networks.
4. Describe the hybrid dynamical system framework proposed by Sanfelice, Goebel and Teel.
5. Describe methods for probabilistic reasoning and decision-making over time, and how this may be applicable to under-ice operations of AUVs.

Paper one:

1. Design of a hybrid translational observer accounting for asynchronous and sporadically available sensor measurements using the framework proposed by Sanfelice, Goebel and Teel.
2. Simulate using MATLAB/Simulink and discuss results.

Paper two:

1. Implementation of altitude estimation and control algorithms for under-ice tracking.
2. Develop a risk-based Bayesian network, allowing for online probabilistic reasoning over the risk of a situation.
3. Extend the Bayesian network to a decision network for online risk-based selection of altitude setpoints, and if necessary, abortion of the mission.
4. Simulate using MATLAB/Simulink and discuss results.

The report shall be written in English and edited as an article collection with a resume in front, in the format of a report. It is supposed that Department of Marine Technology, NTNU, can use the results freely in its research work, unless otherwise agreed upon, by referring to the student's work. The thesis should be submitted by July 12th, 2019.

NTNU Trondheim
Norwegian University of Science and Technology
Department of Marine Technology

Co-supervisor: Professor Ingrid B. Utne

Professor Asgeir J. Sørensen
Supervisor

Abstract

This Master thesis investigates tools and methods for developing more robust autonomy solutions for autonomous underwater vehicles (AUV) in Arctic under-ice operations. AUVs are effective platforms for multi-disciplinary scientific research in the polar oceans. However, operations of AUVs in these areas involve a substantial risk of losing the vehicle. The environment under the sea ice is unstructured and unknown, and is further complicated by harsh environmental conditions and reduced capabilities of navigation sensors.

Under the sea ice AUVs are reliant on an acoustic positioning system, as they are not able to surface for position fixes from a global positioning system (GPS). Position measurements from acoustic positioning systems are noisy and may drop out temporarily. Other navigation sensors, such as pressure gauges and Doppler velocity logs (DVL) may also temporarily drop out, and the signals are obtained at an asynchronous sampling rate. Given the nature of asynchronicity and sporadic availability of the navigational signals, the framework of hybrid dynamical systems is used to design and analyze a sensor-based hybrid observer.

A method for the design of a sensor-based hybrid translational observer for underwater navigation is proposed, accounting for noisy, asynchronous and sporadically available sensor measurements. Here, acceleration measurements are assumed readily available. Position and velocity estimates are updated discretely, asynchronous and sporadically as new measurements are obtained. Between measurements, the estimates are continuously predicted forwards in time by integration of kinematic relationships. High-frequency noisy is filtered by taking a weighted discounted average of a finite number of previous states predicted forwards to the current time. Simulations of a six degree of freedom observer which relies on acceleration, velocity and position measurements are conducted.

There is often a trade-off between the scientific reward of a mission plan and the risk involved. For instance, optical mapping of algae and phytoplankton closer to the surface yields higher quality of the acquired data, however, also increases the risk of losing the vehicle under the ice. By including an online risk model, the vehicle may take calculated risks by weighing the potential rewards of an action and the risk involved.

A method for intelligent risk-based under-ice altitude control for AUVs is presented. An altitude guidance law for following a contour of the ice surface via pitch control using measurements from a Doppler velocity log (DVL) is proposed. Furthermore, an online risk model for probabilistic reasoning of the risk of vehicle loss is developed using the framework of Bayesian networks. This network is extended to a decision network for online autonomous risk-based selection and reselection of the setpoint for the altitude controller, and if necessary, send a signal to abort the mission. This will improve safety and robustness of under-ice operations for AUVs.

Sammendrag

Denne masteroppgaven undersøker verktøy og metoder for å utvikle mer robuste autonomiløsninger for autonome undervannsfarkoster (AUV) i arktiske underisoperasjoner. AUVer er effektive plattformer for tverrfaglig vitenskapelig forskning i polarhavene, men operasjoner av AUVer i disse områdene medfører en betydelig risiko for å miste fartøyet. Miljøet under sjøisen er ustrukturert og ukjent, og er ytterligere komplisert av tøffe miljøforhold og reduserte kapabilitier av navigasjonssensorer.

Under sjøis er AUVer avhengige av et akustisk posisjoneringssystem, da de ikke er i stand til å gå til overflaten for posisjonsoppdateringer fra et globalt posisjoneringssystem (GPS). Posisjonsmålinger fra akustiske posisjoneringssystemer inneholder støy og kan droppe ut midlertidig. Andre navigasjonssensorer, for eksempel trykkmålere og Doppler velocity loger (DVL), kan også midlertidig feile, og signalene innhentes ved en asynkron samplingsfrekvens. I lys av dette, er rammeverket for hybride dynamiske systemer brukt til å designe og analysere en sensorbasert hybrid observer.

En metode for design av en sensorbasert hybrid translasjonsobserver for undervannsnavigering er foreslått, og tar hånd om støyende, asynkrone og sporadisk tilgjengelige sensormålinger. Her antas at akselerasjonsmålinger er til en hver tid tilgjengelig. Posisjons- og hastighetsestimater oppdateres diskret, asynkront og sporadisk når nye målinger fås. Mellom målinger blir estimatene kontinuerlig predikert fremover i tid ved integrasjon av kinematiske forhold. Høyfrekvent støy filtreres ved å ta et vektet diskontert gjennomsnitt av et endelig antall tidligere målinger som predikeres fremover til nåværende tid. Simuleringer av en observer med seks frihetsgrader som er avhengig av akselerasjons-, hastighets- og posisjonsmålinger utføres.

Det er ofte en avveining mellom den vitenskapelige belønningen til en oppdragsplan og den involverte risikoen. Optisk kartlegging av alger og fytoplankton nærmere overflaten gir for eksempel høyere kvalitet på de innhentede dataene, men øker også risikoen for å miste fartøyet under isen. Ved å inkludere en online risikomodell kan fartøyet ta beregnede risikoer ved å veie potensielle fordeler av en handling mot risikoen.

En metode for intelligent risikobasert underisaltitudekontroll for AUVer er presentert. En altitudegaidingslov for å følge en kontur av isunderflaten via pitchkontroll ved hjelp av målinger fra en Doppler velocity log (DVL) er foreslått. Videre er en online risikomodell for probabilistisk resonnering av risikoen for tap av fartøy utviklet ved hjelp av rammeverket for Bayesianske nettverk. Dette nettverket er så utvidet til et avgjørelsesnettverk for online autonom risikobasert utvelgelse av setpunktet til altitudekontrolleren, og hvis nødvendig, sende et signal om å avbryte oppdraget. Dette vil øke sikkerheten og robustheten til underisoperasjoner av AUVer.

Preface

This Master thesis is written during the spring of 2019 as the final part of the Master of Science degree in Marine Technology at the Norwegian University of Science and Technology (NTNU) in Trondheim.

This work is part of the research project UNLOCK (unlocking the potential of autonomous systems and operations through supervisory risk control) at the Centre for Autonomous Operations and Systems (AMOS).

The thesis is edited as a resume with two appended scientific papers. The first paper with title *Sensor-based hybrid translational observer for underwater navigation* is accepted and to be published at the 12$^{\text{th}}$ IFAC conference on Control Applications in Marine Systems (CAMS2019), and the second paper with title *Intelligent risk-based under-ice altitude control for autonomous underwater vehicles* is a draft paper submitted to the OCEANS 2019 Seattle conference.

Until the papers are published, this thesis is for limited circulation.

Acknowledgements

First of all, I would like to thank my supervisor Professor Asgeir J. Sørensen for allowing me to pursue a PhD, and introducing me to the exciting field of marine robotics and ocean polar research. I am truly looking forward to my next years as a PhD candidate under his supervision. I am also grateful for his guidance, support and enthusiasm during my work in this thesis. I would like to thank Dr. Petter Norgren for fruitful discussions on operations of AUVs under ice, as well as providing me with the Arctic AUV simulator and help with setting it up. Many thanks go to Dr. Astrid H. Brodtkorb and Dr. Christoph A. Thieme for patiently reading through the report and the papers, providing assistance with structure and readability, and giving advice.

Lastly, I would like to give a big thank you to my girlfriend Charlotte for being the great person she is.

Jens Einar Bremnes,
July 9, 2019

Contents

List of Figures

List of Tables

Abbreviations

AI Artificial intelligence

AUV Autonomous underwater vehicle

BO Bayesian optimization

CC Chance-constrained

CO Center of origin

CPT Conditional probability table

CTD Conductivity temperature depth

DOF Degree of freedom

DVL Doppler velocity log

GNC Guidance, navigation and control

GNSS Global navigation satellite system

GP Gaussian process

GPS Global positioning system

IMU Inertial measurement unit

INS Inertial navigation system

LBL Long base line

LoA Level of autonomy

LOS Line-of-sight

MBE Multibeam echosounder

MDP Markov decision process

NED North-East-Down

PID Proportional-integral-derivative

POMDP Partially observable Markov decision process

ROV Remotely operated vehicle

SLAM Simultaneous localization and mapping

SNAME Society of Naval Architects and Marine Engineers

USBL Ultra-short base line

UUV Unmanned underwater vehicle

1 Introduction

Autonomous underwater vehicles (AUV) are effective platforms for multi-disciplinary science research and monitoring in the polar oceans. However, operations in polar oceans and under sea ice involve significant risk to the vehicle. The aim of this thesis is to investigate tools and methods for developing more robust autonomy solutions for AUVs in Arctic operations, with focus on navigation, guidance and control, as well as online reasoning and decision-making.

This thesis is twofold. The first part is an introduction with background and motivation for research in the polar oceans and how AUVs are used as sensor platforms, followed by relevant background theory and mathematical modeling. The second part consists of two scientific papers, where the first is related to navigation, and the second to intelligent risk-based control for under-ice operations of AUVs.

1.1 Background and motivation

The Arctic has seen a dramatic decrease in sea-ice extent, and greenhouse gases emitted through human activity is thought to be the main cause. Recorded Arctic sea-ice extent in October shows a decline of 9.3% per decade [1], and the mean Arctic sea-ice thickness has decreased from 3.64 m to 1.89 m in the period 1980-2008 [2]. Further, the rate of warming in the Arctic is more than twice the rate of globally averaged warming [3]. Ice has higher albedo than water and land surfaces, i.e. is more reflective in terms of solar radiation. The decrease in sea-ice extent is thus a positive feedback loop; as global ice cover decreases, the reflectivity of Earth's surface decreases, more incoming solar radiation is absorbed by the surface, resulting in increased global temperatures, and hence, even more ice melts [4]. Figure 1 shows a map of the nations with land within the Arctic region.

Traditionally, the Arctic marine ecology has been treated as a biological desert, as it was believed that the absence of light reduces biological processes to a minimum. In Berge et al. [5], an entirely different view is presented, where high levels of biological activity were recorded at Arctic latitudes during the darkest months. Increased understanding of the Arctic ecology and the effects of the changing climate in the Arctic will be of importance for future environmental management.

This motivates using autonomous underwater vehicles (AUVs) as sensor platforms for Arctic marine research. AUVs are less dependent on support vessels and will therefore reduce the costs of Arctic operations. They also provide high spatial resolution data over large areas [7], are less vulnerable to weather conditions, reduce exposure of crew to cold climate conditions and enables accessibility to areas previously too difficult to access.

However, operations at Arctic latitudes are complicated by harsh environmental conditions, severely limited communication, as well as the possibility of drifting sea ice entering the operational area. As AUV operations extend further under the ice, robust control, autonomous decision-making and online risk management becomes increasingly important.

Figure 1: A map of the nations with land within the Arctic region. Image courtesy of the U.S. state department [6].

1.2 Towards autonomous systems

Increasing the level of autonomy in control systems may improve overall efficiency, safety and operation window, and may reduce cost of operation. In the case of AUVs, increasing the level of intelligence will make the survey and mapping operations more efficient, either by optimizing the available range or optimizing the entire survey including prioritizing the instruments [7].

1.2.1 Definition of agent

When talking about autonomous entities, the word *agent* is frequently used. An agent can be defined as anything that can perceive and influence its environment by using sensors and actuators [8]. In general, agents can be classified into four different types, in order of increasing generality:

- **Simple reflex agents**: These agents select actions on the basis of the current percept, ignoring the rest of the percept history. In other words, they are *memoryless* agents.
- **Model-based reflex agents**: By including some sort of internal state that depends on the percept history, the agent is to some extent able to reflect on some of the unobserved aspects of the current state.
- **Goal-based agents**: Goal-based agents have some *goal information*, and utilizes searching and planning in order to achieve its goal(s). They are more flexible because the knowledge that supports its decisions is represented explicitly and can be modified.

- **Utility-based agents**: By utilizing utility functions, the agent is able to search and plan for a set of actions that maximizes the agent's utility. Utilities provide a spectrum of performance, rather than the crude binary distinctions provided by goals.

By increasing the generality, the agent's flexibility and possibly performance also increases. However, it also increases the complexity and uncertainty of the agent's decision-making.

1.2.2 Definition of autonomy

The definition of the word *autonomy* in the robotics and vehicle communities can be rather vague. Some argue that an autonomous vehicles require that the vehicles are unmanned. Others emphasizes the ability of self-decision based on situational awareness, ability of handling unexpected events and operating in unknown environments. Some examples of how *autonomous vehicles* have been defined in the literature are:

- To avoid a prolonged debate over how much "intelligence" is required for a vehicle to be considered "autonomous," the committee elected to include within the scope of this report all relevant vehicles that do not have a human onboard [9].
- Capable of operating without operator input for extended periods of time. Implicit in this description is the requirement that the UUV's sortie accomplishes its assigned goal and makes the appropriate rendezvous for a successful recovery [10].
- A system's or sub-systems's own ability of integrated sensing, perceiving, decision-making and acting, to achieve its goals as assigned by its human operator(s) through designed human-machine interface.[11].

Rather than saying that an agent is autonomous or not, it may be more reasonable to describe autonomy as a spectrum of autonomy levels; an agent can be somewhere between non-autonomous, partially autonomous and fully-autonomous. The Uninhabited Combat Air Vehicle Program defines four levels of autonomy [12], which later was modified by [11] as follows:

1. **Automatic operation (remote control)** means that the system operates automatically. The human operator directs and controls all high-level mission planning functions, often preprogrammed.
2. **Management by consent (teleoperation)** means that the system automatically makes recommendations for mission actions related to specific functions, and the system prompts the human operator at important points in time for information or decisions. At this level the system may have limited communication bandwidth including time delay, due to i.e. distance. The system can perform many functions independently of human control when delegated to do so.
3. **Semi-autonomous (management by exception)** means that the system automatically executes mission-related functions when response times are too short for human intervention. The human may override or change parameters and cancel or redirect actions within defined time lines. The operators attention is only brought to exceptions for certain decisions.

4. **Highly autonomous** means that the system automatically executes mission related functions in an unstructured environment with ability to plan and re-plan the mission. The human may be informed about the progress. The system is independent and "intelligent".

It can be noted that the different levels of autonomy is comparable to the increasing generality of agents, ranging from simple reflex agents to utility-based agent.

1.2.3 Robust autonomy

As the level of autonomy increases in systems, more responsibility in the operation is shifted from human operators to the system itself. Faults, accidents and other hazardous events in operation of autonomous systems may lead to significant economic losses, and in the worst case, human fatalities. Robustness is an important aspect of autonomous systems, and is a central topic of this thesis. In the Cambridge Dictionary [13] robustness is defined as "*the quality of being strong, and healthy or unlikely to break or fail*". Some definitions and descriptions of robust autonomy found in the literature are:

- Robust autonomy describes the ability of an autonomous system to either continue its operation in the presence of faults or safely shut down [14].
- Robust autonomy on the part of software agents requires, at least in part, the ability to deal intelligently with novel and unexpected situations [15].
- Robust autonomous systems will need to be adaptable to changes in the environment and changes in the underlying physical system [16].

As seen, robust autonomy is generally considered as the ability of the system to adapt to and handle changes in the environment, unexpected situations, abnormal events and fault-tolerant control. For mission-critical and safety-critical operations of autonomous systems, robustness needs to be safeguarded - that is, we must ensure that the system has a high degree of dependability in its operation.

Robustness in the control theory community is defined as the control system's ability to perform as specified in the presence of disturbances and modeling errors. Both definitions have clear similarities. Where robust control deals with system performance through control efforts subject to uncertain input disturbances, robust autonomy also deals with how well the system's decision-making capabilities is able to intelligently handle uncertainties in the environment.

1.3 Case study: AUV operations in the Arctic

In this thesis, case studies using the Kongsberg REMUS 100 AUV are presented, where operations under sea ice in the Arctic are investigated. We assume that the AUV operates in an area with pre-installed subsea acoustic positioning system infrastructure consisting of transducers. Oceanographers and marine biologists are interested in collecting data close to the ice surface. Hence, a robust altitude control system for ice surface following is required. Due to the unpredictability and the occasional unavailability of the acoustic position measurements, the vehicle also relies on a robust navigational system. The Arctic under-ice environment is unknown, unstructured and hazardous. Therefore, the

AUV should also be equipped with some artificial intelligence (AI) capabilities allowing for online reasoning and decision-making. Figure 2 shows typical under-ice operations of AUVs where acoustic positioning systems are present.

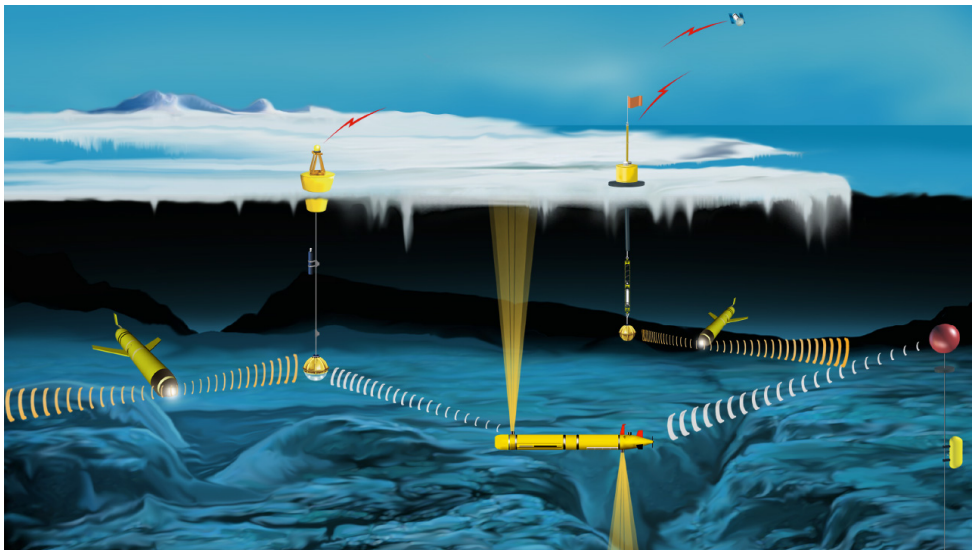

Figure 2: Under-ice operation of AUV with different communication systems. Image courtesy of Woods Hole Oceanographic Institution [17].

1.3.1 Unmanned underwater vehicles

Unmanned underwater vehicles (UUVs) are vehicles able to operate in underwater environments without a human occupant. They are typically divided into two subcategories; remotely operated vehicles (ROVs) and autonomous underwater vehicles (AUVs). ROVs are tethered underwater vehicles, operated remotely by humans onshore or aboard a support vessel, often equipped with manipulator arms for intervention tasks. This thesis will focus on AUVs; untethered vehicles that operates autonomously with minimal human intervention and with limited communication capabilities.

AUVs can provide high spatial and temporal resolution and coverage when gathering data. They may carry sensors that provide unique 3D mapping capabilities. AUV operations are used in several areas and industries such as scientific research, defense, oil and gas, offshore renewable energy and aquaculture. Some applications are oceanography, hydrography, marine biology, marine archeology, mine counter measures, bathymetric surveys and pipeline inspections.

However, operations of AUVs include a substantial risk of vehicle, especially under ice. Also, online control and power supply is limited, which imposes stronger demands to autonomy compared to ROVs.

1.3.2 Sensor capabilities for AUVs

In general, sensors for underwater vehicles can be divided into two categories: payload sensors and navigation sensors.

Payload sensors
Payload sensors are measurement units that are carried by a platform for collecting data either by remote sensing or by direct measurements [7]. Some examples are video cameras for high-resolution images, underwater hyperspectral imagers (UHI), conductivity temperature depth (CTD) sensors, magnetometers and active sonars. CTD sensors measure conductivity, temperature and pressure, which can further be used to calculate the salinity, density and the speed of sound. These are key parameters for oceanography. UHIs are able to quantify colour information at all wave lengths, which can be used to characterize substances, such as chlorophyll and pigments by their reflection spectrum. Magnetometers can be used for localization of shipwrecks in marine archeology. Active sonars, such as multibeam echosounders (MBE), transmit acoustic impulses and measure the reflected signals, which can be used for bathymetric surveys and identification of objects of archeological interest.

Navigation sensors
Navigation sensors are measurement units used for monitoring the motion and location of the vehicle. Due to the degradation of electromagnetic wave signals in underwater environments, GPS is not applicable for underwater navigation. Typically, two types of navigational systems are common in underwater vehicles: inertial navigation systems (INS) and acoustic positioning systems. For acoustic positioning, long base line (LBL) or ultra-short base line (USBL) are typically used. By using a transducer placed on the vehicle, it is able to obtain position measurements through triangulation or quadlateration by communicating with at least three or four transponders, respectively. However, acoustic positioning systems require external subsea infrastructure. The inertial navigation systems use inertial measurement units (IMU), i.e. gyroscopes and accelerometers, in order to provide estimates of the vehicle's position, orientation and linear and angular velocities. However, due to integration of measurement bias, the navigation uncertainty grows unbounded unless position fixes are acquired by either GPS or acoustic positioning systems. Heading sensors, such as magnetic compasses, provide heading estimates for the vehicle, whereas pressure sensors provide an estimate of the vehicle depth. Doppler velocity logs (DVL) measure water current velocities over a depth range using the Doppler effect of sound waves scattered back from particles within the water column. It may also measure the relative velocity and distance to the seabed, which can be used for bottom-tracking. If the AUV is equipped with upwards-looking DVL, it is also be possible to estimate the relative velocity between the AUV and ice surface, as well as the distance.

1.3.3 Risk of autonomous agents in the Arctic marine environment

In order to achieve safe system performance of higher-level autonomy and intelligence in systems operating in the Arctic, supervisory risk control and online risk modelling is required. Autonomous systems must for instance be able to identify and isolate failures and reconfigure to handle any deviations from normal operation [11].

In a risk analysis, the objective is to answer three questions: 1) what can go wrong, 2) what is the likelihood of that happening and 3) what are the consequences. Thus, the risk of a hazardous event e_i can be described by a triplet [18]:

$$r = \{e_i, c_i, q\}|k \tag{1}$$

where c_i is the consequence(s) of e_i, q is a measure of the uncertainty involved, and k

is the background knowledge used for determining e_i, c_i and q. Risk models related to mission success are important for AUVs, as they are costly and may carry expensive payload. According to Utne et al. [11], in operations with high levels of autonomy, risk reduction is completely dependent on a robust and resilient design of the system, but also on an online risk management system. The system should also possess efficient and high integrity machine learning and adaptive functionality.

Operations in the Arctic marine environment offer many unique challenges not found elsewhere. Some of the typical challenges in the Arctic are extremely low temperatures, marine icing, snow, polar lows, dark periods and remoteness [19]. Moving ice may impact the AUV during its operation, and the AUV may in the worst case get stuck under ice. The AUV should not plan to surface in areas with high probability of sea ice, as surfacing in ice may damage the AUV's communication systems and prevent recovery. Additionally, there are navigational challenges at Arctic latitudes. The near vertical magnetic field in the Arctic causes magnetic compasses to become unreliable, whereas the uncertainty of North-seeking gyrocompasses will increase due to the low horizontal component in the rotation of Earth.

1.3.4 Performance, environment, actuators and sensors

An important aspect of autonomous agents is the specification of the task environment, which essentially are the "problems" to which the agents are the "solutions". In Russel et al. [8], the task environment is specified according to the PEAS (performance, environment, actuators, sensors) measure: i) what is the performance measure to which the agent should strive for, ii) what is the environment the agent will face, iii) what kind of actuators does the agent possess, and iv) what kind of sensors does the agent have in order to perceive the environment. The PEAS specification of this case study is:

Performance: The AUV should sample data as close to the ice surface for better data quality, but not at the risk of losing the vehicle.

Environment: The AUV will operate under Arctic sea ice. The under-ice environment is a priori unknown and unstructured. Obstacles, such as icebergs, ice ridges and ice floes may be encountered.

Actuators: The AUV is equipped with propellers for generating surge motion, rudders for generating yaw motion and fins for generating pitch motion. Additionally, a human-machine interface is included for displaying and communicating relevant information to the human operators.

Sensors: For navigation, the AUV is equipped with a GPS, an IMU, a DVL, a transponder and a pressure gauge. For data collection, the AUV is equipped with CTD sensors, an UHI, a MBE and a battery meter. Human operators are also able to communicate to the AUV via the human-machine interface.

1.4 Research questions

The scientific goal of this thesis is to assess methods for robust guidance, navigation, control, reasoning and decision-making of AUVs for Arctic under-ice operations. Specifically, this thesis aims to answer the following questions:

1. How can the AUV navigate relative to the ice surface?

2. How can the altitude of AUVs under the ice be controlled such that it is able to safely follow a contour of the ice surface?

3. How can we design and analyze navigation systems for under-ice operations accounting for noisy, asynchronous and sporadically available sensor measurements?

4. How can we increase the robustness of under-ice operations through online risk modeling and risk control?

These research questions may further be summarized into one question, in which this Master thesis aims to answer:

> How can we increase the robustness of autonomous underwater vehicles in Arctic operations?

1.5 Main contributions

There are two main contributions of this thesis. Firstly, the hybrid system framework proposed by Goebel et al. [20] is investigated for the design of sensor-based observers. Secondly, AI-based methods for reasoning and decision-making under uncertainty are integrated with under-ice altitude control in order to achieve intelligent risk-based control. These contributions are captured by the two appended papers. Below, the individual contributions of the papers are summarized.

Paper 1 : *Sensor-based hybrid translational observer for underwater navigation.* Accepted and to be published at the 12$^{\text{th}}$ IFAC Conference on Control Applications in Marine Systems (CAMS2019), Daejeon, Korea. A sensor-based hybrid translational observer for underwater navigation is designed, accounting for noisy, asynchronous and sporadically available sensor measurements. A method for filtering high-frequency noise is proposed, where the estimated states are obtained by taking a weighted discounted average of a finite number of previous measurements predicted forwards to the current time. Results from simulations are presented to demonstrate the performance of the proposed method.

Paper 2 : *Intelligent risk-based under-ice altitude control for autonomous underwater vehicles.* Draft paper submitted to the OCEANS 2019 Seattle Conference, Seattle, USA. A method for intelligent risk-based under-ice altitude control for AUVs is presented. An altitude guidance law for following a contour of the ice surface is proposed. A desired pitch angle is calculated based on the estimated altitude error and the estimated slope of the ice surface in the vehicle heading direction. Furthermore, a Bayesian network is created for the purpose of online probabilistic reasoning over the current state of risk during operation. This network is then extended to a decision network for online risk-based selection and reselection of the setpoint for the altitude controller. Results from simulations are presented to demonstrate the performance of the method.

1.6 Organization of thesis

The outline of this Master thesis if as follows:

Chapter 2 presents the theories and methods used in the papers more thoroughly. Covered topics include mathematical modeling of AUVs, kinematics, motion control systems, under-ice altitude control, hybrid dynamical systems and probabilistic reasoning and decision-making.

Chapter 3 describes the simulator environment setups used in the two appended papers.

Chapter 4 summarizes the findings and contributions of the two scientific papers, concludes the Master thesis and presents recommendations for further work.

Paper 1 *Sensor-based hybrid translational observer for underwater navigation*

Paper 2 *Intelligent risk-based under-ice altitude control for autonomous underwater vehicles*

Appendix A gives numerical values used for the mathematical models in the simulator.

2 Background and mathematical modeling

In this chapter, background theory used further in this thesis, such as mathematical modelling of AUVs, kinematics, motion control systems, under-ice altitude control, hybrid dynamical systems and probabilistic reasoning and decision-making, is covered.

In the mathematical modelling of AUVs, the notation that complies with the Society of Naval Architects and Marine Engineers (SNAME) for the 6 degree of freedom (DOF) motion components with its corresponding forces and moments has been adapted. For details regarding this notation, see Table 1.

DOF		Forces and moments	Linear and angular velocities	Position and Euler angles
1	translations in the x direction (surge)	X	u	x
2	translations in the y direction (sway)	Y	v	y
3	translations in the z direction (heave)	Z	w	z
4	rotations about the x axis (roll)	K	p	ϕ
5	rotations about the y axis (pitch)	M	q	θ
6	rotations about the z axis (yaw)	N	r	ψ

Table 1: SNAME notation for marine craft

2.1 Kinematics

When analyzing the motion of a marine craft in 6 DOF, it is convenient to define several reference frames. In this thesis, four reference frames have been used:

- **NED** $\{n\}$: The NED (North-East-Down) reference frame $\{n\} = (x^n, y^n, z^n)$ is defined relative to the Earth's reference ellipsoid. In this frame, the x axis points towards true *North*, the y axis points towards true *East* and the z axis points downwards normal to the Earth's surface.
- **BODY** $\{b\}$: The body-fixed reference frame $\{b\} = (x^b, y^b, z^b)$ is a moving coordinate frame fixed to the marine craft. The axes in this frame coincides with the principal axes of inertia.
- **DVL** $\{d\}$: The DVL-frame $\{d\} = (x^d, y^d, z^d)$ is a reference frame fixed to the center of the DVL sensor in the DVL's body-frame.
- **CO** $\{co\}$: The CO-frame $\{co\} = (x^{co}, y^{co}, z^{co})$ is a reference frame parallel with $\{n\}$, but fixed to the center of origin (CO) of the AUV.

In order to transform vectors between the NED-frame and body-frame, Euler angle transformation is used. The linear velocity transformation from $\{b\}$ to $\{n\}$ can be described by three principal rotations about the z, y and x axes by

$$\boldsymbol{R}_b^n(\boldsymbol{\Theta}) = \boldsymbol{R}_{z,\psi}\boldsymbol{R}_{y,\theta}\boldsymbol{R}_{x,\phi} \tag{2}$$

with

$$\boldsymbol{R}_{x,\phi} = \begin{bmatrix} 1 & 0 & 0 \\ 0 & c\psi & -s\psi \\ 0 & s\psi & c\psi \end{bmatrix}, \ \boldsymbol{R}_{y,\theta} = \begin{bmatrix} c\theta & 0 & s\theta \\ 0 & 1 & 0 \\ -s\theta & 0 & c\theta \end{bmatrix}, \ \boldsymbol{R}_{z,\psi} = \begin{bmatrix} c\psi & -s\psi & 0 \\ s\psi & c\psi & 0 \\ 0 & 0 & 1 \end{bmatrix} \tag{3}$$

where $s \cdot = \sin(\cdot)$ and $c \cdot = \cos(\cdot)$. Further, the angular velocity transformation from $\{b\}$ to $\{n\}$ is given by

$$\dot{\boldsymbol{\Theta}} = \boldsymbol{T}_{\Theta}(\boldsymbol{\Theta})\boldsymbol{\omega} \tag{4}$$

with

$$\boldsymbol{T}_{\Theta}(\boldsymbol{\Theta}) = \begin{bmatrix} 1 & s\phi t\theta & c\phi t\theta \\ 0 & c\phi & -\phi \\ 0 & s\phi/c\theta & c\phi/c\theta \end{bmatrix} \tag{5}$$

where $t \cdot = \tan(\cdot)$. Note that $\boldsymbol{T}_{\Theta}(\boldsymbol{\Theta})$ has a singularity for $\theta = \pm 90°$. The position and orientation of the AUV are given in $\{n\}$ as

$$\boldsymbol{\eta} = \begin{bmatrix} \boldsymbol{p} & \boldsymbol{\Theta} \end{bmatrix}^T = \begin{bmatrix} N & E & D & \phi & \theta & \psi \end{bmatrix}^T \in \mathbb{R}^6. \tag{6}$$

The linear and angular velocities of the AUV are given in $\{b\}$ as

$$\boldsymbol{\nu} = \begin{bmatrix} \boldsymbol{v} & \boldsymbol{\omega} \end{bmatrix}^T = \begin{bmatrix} u & v & w & p & q & r \end{bmatrix}^T \in \mathbb{R}^6. \tag{7}$$

The kinematic relationship between the Earth-fixed velocities and the body-fixed velocities can thus be expressed by

$$\dot{\boldsymbol{\eta}} = \boldsymbol{J}_{\Theta}(\boldsymbol{\eta})\boldsymbol{\nu} \tag{8}$$

where

$$\boldsymbol{J}_{\Theta}(\boldsymbol{\eta}) = \begin{bmatrix} \boldsymbol{R}_b^n(\boldsymbol{\Theta}) & \boldsymbol{0}_{3\times 3} \\ \boldsymbol{0}_{3\times 3} & \boldsymbol{T}_{\Theta}(\boldsymbol{\Theta}) \end{bmatrix}. \tag{9}$$

2.1.1 DVL kinematics

The AUV is equipped with an upwards-looking DVL with four beams in a Janus configuration. Numbering of the DVL beams are depicted in Figure 3 below. Each DVL beam has an offset $\gamma_j = \beta_j = \pm 20°$ along the vehicle's longitudinal and transversal direction, respectively.

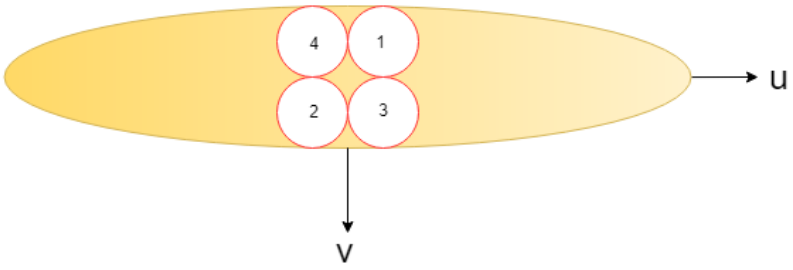

Figure 3: Numbering of DVL beams. u points in positive surge direction, and v points in positive sway direction.

The j^{th} beam of the DVL can in the dvl-frame {d} be expressed as

$$\boldsymbol{r}_{dvl,j}^d = \begin{bmatrix} x_j^d \\ y_j^d \\ a_j^d \end{bmatrix} = r_{dvl,j} \begin{bmatrix} \sin(\gamma_j)\cos(\beta_j) \\ \sin(\gamma_j)\sin(\beta_j) \\ -\cos(\gamma_j) \end{bmatrix} \tag{10}$$

where $r_{dvl,j} = ||\boldsymbol{r}_{dvl,j}^d||_2$ is the range of the j^{th} beam, γ_j is the j^{th} beam's offset angle from the z axis, and β_j is the j^{th} beam's offset angle from the x axis. This is transformed and shifted to the body-fixed frame $\{b\}$ in (11a), and further transformed to $\{n\}$ in (11b):

$$\boldsymbol{r}_{dvl,j}^b = \boldsymbol{R}_d^b(\boldsymbol{\Theta}_{bd})\boldsymbol{r}_{dvl,j}^d + \boldsymbol{r}_{dvl/b}^b \tag{11a}$$

$$\boldsymbol{r}^n_{dvl,j} = \boldsymbol{R}^n_b(\boldsymbol{\Theta})\boldsymbol{r}^b_{dvl,j} \tag{11b}$$

where $\boldsymbol{r}^b_{dvl/b}$ is the vector from the CO of the AUV to the center of the DVL expressed in $\{b\}$, and $\boldsymbol{\Theta}_{bd}$ is the orientation of $\{d\}$ relative to $\{b\}$.

Thus, we have obtained four vectors from the CO of the AUV to the ice surface in $\{n\}$:

$$\boldsymbol{r}^n_{dvl,j} = \begin{bmatrix} x^n_j \\ y^n_j \\ a^n_j \end{bmatrix}, \ j = 1, 2, 3, 4. \tag{12}$$

2.1.2 Altitude kinematics

Definition 1. The altitude of the AUV is the z component of the vector from the CO of the AUV to the point on the ice surface with the same horizontal coordinates as the CO of the AUV expressed in $\{n\}$.

This definition of altitude might be slightly misleading, as the term altitude most often is used as the length of the vector from the CO of a vehicle to the point on the sea bed with the same horizontal coordinates as the CO of the vehicle. This will, however, not distinguish between the direction of the vector. Note that the altitude under the ice with this thesis' definition will be negative.

Let $z_{ice} = f(x, y)$ denote the depth of the ice surface at position (x, y). The altitude can then be expressed as

$$a = f(x, y) - z. \tag{13}$$

2.1.3 Altitude rate of change

The altitude rate of change can be found by differentiating (13) with respect to time. Using partial differentiation and the chain rule, this becomes

$$\dot{a} = \frac{\partial f}{\partial x}\frac{dx}{dt} + \frac{\partial f}{\partial y}\frac{dy}{dt} - \frac{dz}{dt}. \tag{14}$$

This may be simplified by introducing an expression for the submerged ice as a surface given by the equation

$$F(x, y, z) = f(x, y) - z = 0, \quad \frac{\partial F}{\partial t} = 0 \tag{15}$$

where F is a time-invariant function with continuous first-order partial derivatives. In general, F is an unknown function, however, only the gradient of F is of importance. The gradient is, evaluated at the position of the AUV, given by

$$\nabla F(\boldsymbol{p}) = \left[\left.\frac{\partial f}{\partial x}\right|_{\boldsymbol{p}}, \left.\frac{\partial f}{\partial y}\right|_{\boldsymbol{p}}, -1 \right]. \tag{16}$$

The expression for the altitude rate of change (14) can then be rewritten as [21]

$$\begin{aligned}\dot{a} &= \nabla F(\boldsymbol{p}) \cdot \dot{\boldsymbol{p}} \\ &= \left[\left.\frac{\partial f}{\partial x}\right|_{x_p,y_p}, \left.\frac{\partial f}{\partial y}\right|_{x_p,y_p}, -1 \right] \boldsymbol{R}_b^n(\boldsymbol{\Theta}) \begin{bmatrix} u \\ v \\ w \end{bmatrix}.\end{aligned} \tag{17}$$

2.2 Kinetics

A general 6 DOF kinematic equation of motion can be expressed with Fossen's robot-like vectorial model for marine craft [22]:

$$\begin{aligned}\dot{\boldsymbol{\eta}} &= \boldsymbol{J}_\Theta(\boldsymbol{\eta})\boldsymbol{\nu} \\ \boldsymbol{M}\dot{\boldsymbol{\nu}}_r + \boldsymbol{C}(\boldsymbol{\nu}_r)\boldsymbol{\nu}_r + \boldsymbol{D}(\boldsymbol{\nu}_r)\boldsymbol{\nu}_r + \boldsymbol{g}(\boldsymbol{\eta}) &= \boldsymbol{\tau}\end{aligned} \tag{18}$$

where $\boldsymbol{\nu}_r$ is the relative body-fixed velocities, $\boldsymbol{M} = \boldsymbol{M}_{RB} + \boldsymbol{M}_A$ is the rigid-body inertia and added mass matrix, $\boldsymbol{C}(\boldsymbol{\nu}_r) = \boldsymbol{C}_{RB} + \boldsymbol{C}_A$ is the Coriolis and centripetal matrix due to the rotation of {b} about the inertial frame {n}, $\boldsymbol{D}(\boldsymbol{\nu}_r)$ is the hydrodynamic damping matrix and $\boldsymbol{g}(\boldsymbol{\eta})$ are the restoring forces and moments. The generalized control forces expressed in {b} are given as

$$\boldsymbol{\tau} = \begin{bmatrix} X_p & Y_r & Z_s & K_p & M_s & N_r \end{bmatrix}^T \in \mathbb{R}^6. \tag{19}$$

Here, the subscript p denotes the propeller, r the rudder fins and s the stern fins of the AUV. The force in surge and moment in roll due to the propeller have been derived by Carlton [23], and are given as

$$X_p = K_T \rho D_{prop}^4 n|n| \tag{20}$$

$$K_p = K_Q \rho D_{prop}^5 n|n| \tag{21}$$

where K_T and K_Q are the thrust and torque coefficients, respectively, D_{prop} is the propeller diameter and n is the propeller shaft speed. The control surfaces, i.e. the forces and moments from the rudder and stern fins, have been derived by Prestero [24], and are given as

$$Y_r = \frac{1}{2}\rho C_{L,\alpha} S_{fin}[u^2\delta_r - uv - x_{fin}(ur)] \tag{22}$$

$$Z_s = -\frac{1}{2}\rho C_{L,\alpha} S_{fin}[u^2\delta_s + uw - x_{fin}(uq)] \tag{23}$$

$$M_s = \frac{1}{2}\rho C_{L,\alpha} S_{fin} x_{fin}[u^2\delta_s + uw - x_{fin}(uq)] \tag{24}$$

$$N_r = \frac{1}{2}\rho C_{L,\alpha} S_{fin} x_{fin}[u^2\delta_r - uv - x_{fin}(ur)] \tag{25}$$

where ρ is the density of water, $C_{L,\alpha}$ is the fin lift coefficient estimated from an empirical formula as function of the angle of attack α, S_{fin} is the fin area and x_{fin} is the x-coordinate of the fin with respect to the CO. The control variables δ_s and δ_r are the stern and rudder

fin angles relative to the x axis in $\{b\}$, respectively.

The three control variables, one for speed control, one for pitch control and one for heading control, can thus be described by

$$\xi = \begin{bmatrix} n & \delta_s & \delta_r \end{bmatrix}^T. \tag{26}$$

2.3 Environmental modelling

As the AUV operates under water, it will not be subject to any wind forces. It is also assumed that the effects of wave-induced hydrodynamic pressure under the sea ice are negligible. Therefore, the only environmental loads considered in this thesis are those from the ocean current. In the Arctic, ice may take many forms, and this creates obstacles that the AUV should avoid. A brief ice glossary is also included in this section.

2.3.1 Ocean current

It assumed that the ocean current has constant speed V_c, is irrotational and does not have any vertical component. The ocean current velocity vector in $\{b\}$ can thus be expressed as

$$\boldsymbol{\nu}_c = \begin{bmatrix} V_c \cos(\psi_c) & V_c \sin(\psi_c) & 0 & 0 & 0 & 0 \end{bmatrix}^T \in \mathbb{R}^6 \tag{27}$$

where $\psi_c = \beta_c + \psi$ is the current direction relative to the heading of the AUV and β_c is the current direction in $\{n\}$.

2.3.2 Ice

In the Arctic, an AUV will face ice of different types. This will create obstacles for the AUV to avoid. An extensive ice glossary is provided by Environment and Climate Change Canada in [25]. Some of the ice types the AUV may meet in the Arctic are:

- **Icebergs**: "A massive piece of ice of greatly varying shape, protruding 5 m or more above sea level, which has broken away from a glacier and which may be afloat or aground. They may be described as tabular, domed, pinnacled, wedged, drydocked or blocky. Sizes of icebergs are classed as small, medium, large and very large."
- **Ice ridges**: "A line or wall of broken ice forced up by pressure. It may be fresh or weathered. The submerged volume of broken ice under a ridge, forced downwards by pressure, is termed an ice keel."
- **Level ice**: "Ice unaffected by deformation."
- **Ice floes**: "Any relatively flat piece of ice 20 m or more across. Floes are subdivided according to horizontal extent as follows: 1) Small: 20-100 m across, 2) Medium: 100-500 m across, 3) Big: 500-2,000 m across, 4) Vast: 2-10 km across, 5) Giant: Greater than 10 km across."
- **Slush**: "Snow which is saturated and mixed with water on land or ice surfaces or as a viscous floating mass in water after a heavy snowfall."

2.4 Control systems

In the following section, background theory on motion control system architectures is presented, including details regarding the implemented control and guidance systems.

A motion control system is usually constructed as three independent blocks, namely the *guidance*, *navigation* and *control* (GNC) blocks [22], see Figure 4. The task of the guidance block is to continuously compute the reference positions, velocities and accelerations of the vehicle. The task of the navigation block is to determine the vehicle's position and orientation, as well as linear and angular velocities and accelerations. This is done by processing raw data from motion sensors such as global navigation satellite systems (GNSS) and inertial measurement units (IMU). The observer in the navigation block is responsible of filtering out undesired frequencies, reconstructing unmeasured states and prediction of states when signals are lost (dead reckoning). The task of the control block is to determine the necessary control forces and moments in order to satisfy the control objective as assigned by the guidance system. Further, it allocates efforts to each actuator in order to achieve the desired control forces and moments.

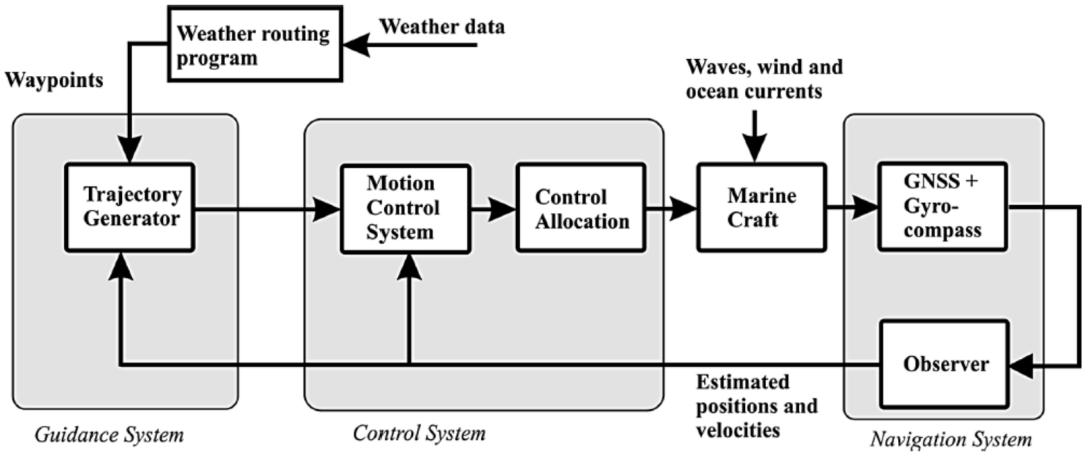

Figure 4: GNC signal flow. Image courtesy of Fossen [22].

2.4.1 Control system architectures

A general system architecture for autonomous systems combining reactive and deliberate control is given in Figure 5. As seen, the architecture can be divided into three layers, from high to low level:

1. **Mission planning layer**: In the mission planner level, the mission objective is defined and planned (and possibly re-planned). Risk reducing preventive measures are of importance.

2. **Guidance and optimization layer**: Here, the waypoints and reference commands to the controller are handled. Optimized model-predictive control may also be used accounting for varying references and forecasted variations in environmental and operational conditions.

3. **Control execution layer**: In this layer, the plant control, actuator control and navigation occur at the highest bandwidth.

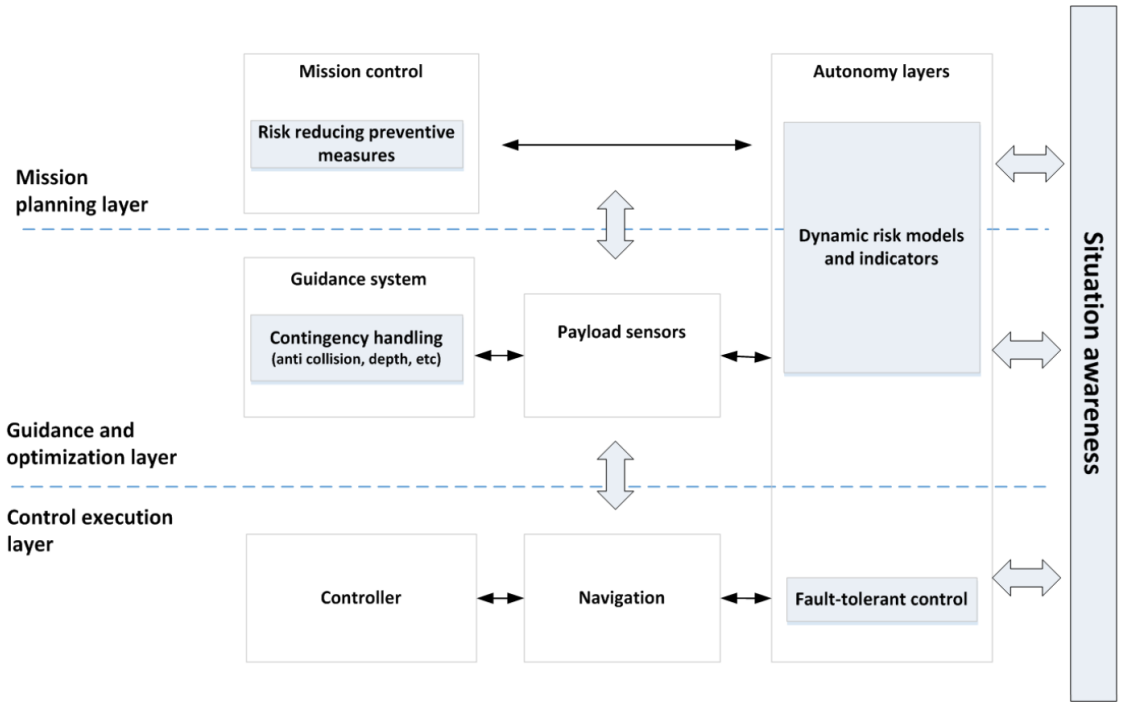

Figure 5: System architecture for autonmous systems combining reactive and deliberate control. Image couresty of Utne et al. [11].

2.4.2 Motion control system for the AUV

The implemented motion control system in the simulator consists of three individual controllers; a speed controller, a depth controller and a heading controller.

The speed controller is a PI controller on the vehicle speed error. The desired shaft speed is found by mapping the desired vehicle speed to shaft revolutions per minute:

$$n = k_{p,n}(U - U_d) + k_{i,n} \int_0^t (U - U_d)dt \tag{28}$$

In the depth controller, the desired depth is achieved by altering the pitch of the vehicle. This is done with two separate feedback loops. The first loop is a proportional-integral (PI) controller on the depth error, which generates a desired pitch angle. The second loop is a proportional-integral-derivative (PID) controller that tracks the desired pitch by controlling the stern planes of the AUV. The depth controller can be expressed as

$$\begin{aligned} \theta_d &= k_{p,\theta}(z - z_d) + k_{i,\theta} \int_0^t (z - z_d) \\ \delta_s &= k_{p,\delta_s}(\theta - \theta_d) + k_{i,\delta_s} \int_0^t (\theta - \theta_d)dt + k_{d,\delta_s} q. \end{aligned} \tag{29}$$

The heading controller is a PID controller that tracks the desired heading by controlling the rudder fins of the AUV:

$$\delta_r = k_{p,\delta_r}(\psi - \psi_d) + k_{i,\delta_r} \int_0^t (\psi - \psi_d)dt + k_{d,\delta_r} r \tag{30}$$

In all three controllers, the setpoints are first passed through reference models in order to avoid excessive changes in the control commands. A block diagram of the motion control system is depicted in Figure 6 below.

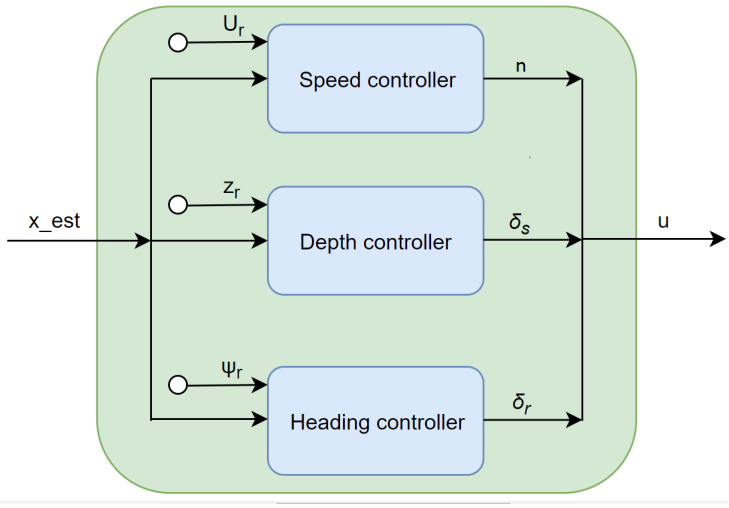

Figure 6: Block diagram showing details of the motion control system. Here, z_r denotes the reference depth, ψ_r the reference heading, U the speed, δ_s the aileron angle and δ_r the rudder angle. The system input x_est is the estimated states and the system output u is a vector containing the desired control actuations.

2.4.3 Guidance system for the AUV

The implemented guidance system in the simulator is a line-of-sight (LOS) lookahead-based steering law for path following of piece-wise linear segments composed of a list of 3D waypoints $WP_k = \begin{bmatrix} x_k & y_k & z_k \end{bmatrix}^T$. The steering law calculates a desired course angle $\chi_d(t)$ online, which is then sent as a reference course to the low-level heading controller. The desired depth is acquired using a separate depth controller. The desired course angle χ_d can be expressed as the sum of the *path-tangential angle* χ_p and the *velocity-path relative angle* χ_r:

$$\chi_d = \chi_p + \chi_r(e). \tag{31}$$

The path-tangential angle $\chi_p = \alpha_k$ is the angle of the linear path segment relative to the NED frame, which can be expressed as

$$\alpha_k := \text{atan2}(y_{k+1} - y_k, x_{k+1} - x_k). \tag{32}$$

The velocity-path relative angle χ_r ensures that the velocity is directed toward an intersection point on the path, some lookahead distance $\Delta(t) > 0$ ahead of the vehicle. This can be expressed as

$$\chi_r(e) := \arctan\left(\frac{-e}{\Delta}\right) \tag{33}$$

where $e(t)$ is the cross-track error normal to the path. The cross-track error is found from

$$e(t) = -[x(t) - x_k]\sin(\alpha_k) + [y(t) - y_k]\cos(\alpha_k). \tag{34}$$

This guidance scheme ensures that the vehicle is forced to converge to the path, i.e. $\lim_{t\to\infty} e(t) = 0$. Further, a switching mechanism is included such that the next waypoint is chosen if the vehicle lies within a *circle of acceptance* with radius R_{k+1} around (x_{k+1}, y_{k+1}). In other words, if the vehicle position (x, y, z) at time t satisfies

$$[x_{k+1} - x(t)]^2 + [y_{k+1} - y(t)]^2 \leq R_{k+1}^2, \tag{35}$$

the next waypoint $(x_{k+1}, y_{k+1}, z_{k+1})$ should be selected. For details regarding this guidance law, the reader is referred to Fossen [22].

2.5 Altitude estimation

In this section, altitude estimation for under-ice applications using a methodology inspired by Dukan et al. [21], originally developed for approximation of the sea floor geometry, is presented. Using four DVL beams, the geometry of the ice surface above the AUV is approximated as a linear surface.

In the simplified case where the DVL is located at the CO of the AUV, the vectors $\boldsymbol{r}_{dvl,j}^b = \boldsymbol{r}_{dvl,j}^d$ will be equal. Thus, the j^{th} DVL measurement can in $\{b\}$ be expressed as

$$\boldsymbol{r}_{dvl,j}^b = r_{dvl,j} \begin{bmatrix} \sin(\gamma_j)\cos(\beta_j) \\ \sin(\gamma_j)\sin(\beta_j) \\ -\cos(\gamma_j) \end{bmatrix}. \tag{36}$$

2.5.1 Local ice surface approximation

A local approximation of the ice surface geometry may be given by a linear surface $f(x, y) = a + bx + cy$, in which three points are required. The j^{th} local approximation of the ice surface $\hat{f}_j^{co} = a_j + b_j x + c_j y$ in $\{co\}$ can be found by solving the linear system [21]

$$\begin{bmatrix} 1 & x_j^n & y_j^n \\ 1 & x_{j+1}^n & y_{j+1}^n \\ 1 & x_{j+2}^n & y_{j+2}^n \end{bmatrix} \begin{bmatrix} a_j \\ b_j \\ c_j \end{bmatrix} = \begin{bmatrix} a_j^n \\ a_{j+1}^n \\ a_{j+2}^n \end{bmatrix} \tag{37}$$

where $\hat{f}_j^{co}$ is the ice surface geometry in $\{co\}$, and $\boldsymbol{r}_{dvl,j}^n = [x_j^n, y_j^n, a_j^n]$ is the j^{th} DVL beam vector in $\{n\}$. The corresponding approximated sea floor gradient vector is given by

$$\nabla \hat{F}_j = \left[\left.\frac{\partial \hat{f}_j}{\partial x}\right|_{\boldsymbol{p}}, \left.\frac{\partial \hat{f}_j}{\partial y}\right|_{\boldsymbol{p}}, -1 \right] = [b_j, c_j, -1]. \tag{38}$$

In order to improve the accuracy of the ice surface geometry approximation, least squares method regression utilizing all four DVL beams is used. The ice surface is then at each time step approximated as a linear surface $\hat{f}^{co}(x, y) = a_m + bx + cy$ by solving

$$[a_m, b, c] = \text{argmin}_{a_m,b,c} \sum_{i=1}^{4} [a_i^n - (a_m + bx_i^n + cy_i^n)]^2. \tag{39}$$

This is done by including the 4^{th} DVL measurement in the linear system in (37). Thus, we get a new linear system $\boldsymbol{Ax} = \boldsymbol{b}$:

$$\begin{bmatrix} 1 & x_1^n & y_1^n \\ 1 & x_2^n & y_2^n \\ 1 & x_3^n & y_3^n \\ 1 & x_4^n & y_4^n \end{bmatrix} \begin{bmatrix} a_m \\ b \\ c \end{bmatrix} = \begin{bmatrix} a_1^n \\ a_2^n \\ a_3^n \\ a_4^n \end{bmatrix}. \tag{40}$$

The solution $\boldsymbol{x} = [a_m, b, c]^T$ of (39) is found by solving the system $\boldsymbol{A}^T\boldsymbol{Ax} = \boldsymbol{A}^T\boldsymbol{b}$. The approximated altitude of the AUV is then a_m, and the approximated ice surface gradient vector is

$$\nabla\hat{F} = \left[\left.\frac{\partial\hat{f}}{\partial x}\right|_{\boldsymbol{p}}, \left.\frac{\partial\hat{f}}{\partial y}\right|_{\boldsymbol{p}}, -1 \right] = [b,\ c,\ -1]. \tag{41}$$

The approximated altitude rate of change α_m is then given by

$$\alpha_m = \left[\left.\frac{\partial\hat{f}}{\partial x}\right|_{\boldsymbol{p}}, \left.\frac{\partial\hat{f}}{\partial y}\right|_{\boldsymbol{p}}, -1 \right] \boldsymbol{R}_b^n(\hat{\boldsymbol{\Theta}}) \begin{bmatrix} \hat{u} \\ \hat{v} \\ \hat{w} \end{bmatrix} \tag{42}$$

where $\hat{(\cdot)}$ denotes an estimated value. In this thesis, we assume that the attitude and velocity of the vehicle are known, i.e. $\hat{\boldsymbol{\Theta}} = \boldsymbol{\Theta}$ and $\hat{\boldsymbol{v}} = \boldsymbol{v}$.

2.5.2 Altitude observer

When using only the method explained in section 2.5.1, where a local ice surface approximation was done, discontinuous altitude estimates will be obtained. This is because the four DVL beams are affected by noise, and may experience sudden drops in values, e.g. when meeting a wall of ice or measuring roughness in the ice surface. In order to ensure a continuous and smooth estimated altitude suitable for feedback, an altitude observer using a Kalman filter is implemented. The inputs to the altitude observer are the approximated altitude a_m and the approximated altitude rate of change α_m.

The discrete-time measured altitude $a_m(k)$ and altitude rate of change $\alpha_m(k)$ at time step k can be expressed as the sum of the true value and some noise processes $v(k)$ and $w(k)$:

$$a_m(k) = a(k) + v(k) \tag{43a}$$

$$\alpha_m(k) = \dot{a}(k) + w(k) \tag{43b}$$

Here, a and $\dot{a}$ represent the true altitude and altitude rate of change, respectively. Using Euler integration with time step h, the discrete-time control plant model can be expressed as:

$$\begin{aligned} a(k+1) &= a(k) + \dot{a}(k)h \\ &= a(k) + \alpha_m(k)h - w(k)h \end{aligned} \tag{44}$$

$$\begin{aligned} y(k) &= a_m(k) \\ &= a(k) + v(k) \end{aligned}$$

This can be reformulated to the notation used in Fossen [22]:

$$\begin{aligned} x(k+1) &= \Phi x(k) + \Delta u(k) + \Gamma w(k) \\ y &= Hx(k) + v(k) \end{aligned} \tag{45}$$

where $x = a_m$, $u = \alpha_m$, $\Phi = 1$, $\Delta = h$, $\Gamma = -h$, $H = 1$ and h is the timestep. Furthermore, a discrete Kalman filter copying the dynamics of (45) is implemented. The algorithm of a general discrete-time Kalman filter is given as:

Predictor:

$$\begin{aligned} \hat{x}(k) &= \bar{x}(k) + K(k)[y(k) - H(k)\bar{x}(k)] \\ \hat{P}(k) &= [I - K(k)H(k)]\bar{P}(k)[I - K(k)H(k)]^T + K(k)R(k)K^T(k) \end{aligned} \tag{46}$$

Update

$$\begin{aligned} K(k) &= \bar{P}(k)H^T(k)[H(k)\bar{P}(k)H^T(k) + R(k)]^{-1} \\ \bar{x}(k+1) &= \Phi(k)\hat{x}(k) + \Delta(k)u(k) \\ \bar{P}(k+1) &= \Phi(k)\bar{P}(k)\Phi^T(k) + \Gamma(k)Q(k)\Gamma^T(k) \end{aligned} \tag{47}$$

where $K(k)$ denotes the Kalman gain, $\hat{x}(k)$, $\bar{x}(k)$, $\hat{P}(k)$ and $\bar{P}(k)$ denote the apriori and aposteriori state estimates and error covariances, respectively, and Q and R denote the process and measurement covariance.

2.6 Altitude control

The main control objective of altitude control is for the vehicle to follow a contour of the ice surface with a constant desired altitude. We propose a line-of-sight (LOS) guidance law with lookahead-based steering in the vertical plane, where the vehicle pitch is controlled in order to obtain the desired altitude.

We want to do a prediction of the change in the ice depth in the vehicle heading direction along a lookahead distance Δ_z, and utilize this in the guidance law. The approximated slope of the ice surface in the heading direction is given as

$$\varpi = \left.\frac{\partial \hat{f}_\psi}{\partial x}\right|_{\boldsymbol{p}} = [1,0,0]\boldsymbol{R}_{z,\hat{\psi}}^{-1}(\hat{\psi}) \left[\left.\frac{\partial \hat{f}}{\partial x}\right|_{\boldsymbol{p}}, \left.\frac{\partial \hat{f}}{\partial y}\right|_{\boldsymbol{p}}, 0 \right]^T \tag{48}$$

where $\boldsymbol{R}_{z,\hat{\psi}}^{-1}(\hat{\psi})$ is the principal rotation matrix about the z axis from $\{n\}$ to $\{b\}$. The first-order prediction of the ice depth change along Δ_z is then calculated as $\varpi\Delta_z$. Because the approximated ice surface slope may ϖ may differ from the real ice surface slope and may contain high values of noise, one might downscale the effect that the prediction will have in the guidance law. The downscaled ice surface slope used in the guidance law is given as

$$\varpi_s = [k_{dive}, k_{ascend}] \begin{bmatrix} \text{sat}^+(\varpi) \\ \text{sat}^-(\varpi) \end{bmatrix} \tag{49}$$

where $k_{dive}, k_{ascend} \in [0, 1]$ are constant parameters determining the downscale factor of positive and negative ice surface slopes, respectively, and

$$\text{sat}^+(s) = \begin{cases} x, & \text{if } x > 0 \\ 0, & \text{otherwise,} \end{cases} \qquad \text{sat}^-(s) = \begin{cases} x, & \text{if } x < 0 \\ 0, & \text{otherwise} \end{cases}$$

are saturation functions only letting through positive and negative numbers, respectively. The motivation for using two different downscale parameters, is that one may wish that the vehicle is more sensitive to positive slopes as they impose a probability of colliding with the ice, i.e. choose the factors such that $k_{dive} \geq k_{ascend}$.

The proposed altitude guidance law is given by

$$\begin{aligned} \theta_d :&= -\arctan\left(\frac{\hat{a} - a_d + \varpi_s \Delta_z}{\Delta_z}\right) \\ &= -\arctan\left(\frac{\hat{a} - a_d}{\Delta_z} + \varpi_s\right) \end{aligned} \tag{50}$$

where θ_d is the desired pitch, which is sent as input to a reference model, and then a pitch controller. The altitude LOS guidance law is depicted in Figure 7.

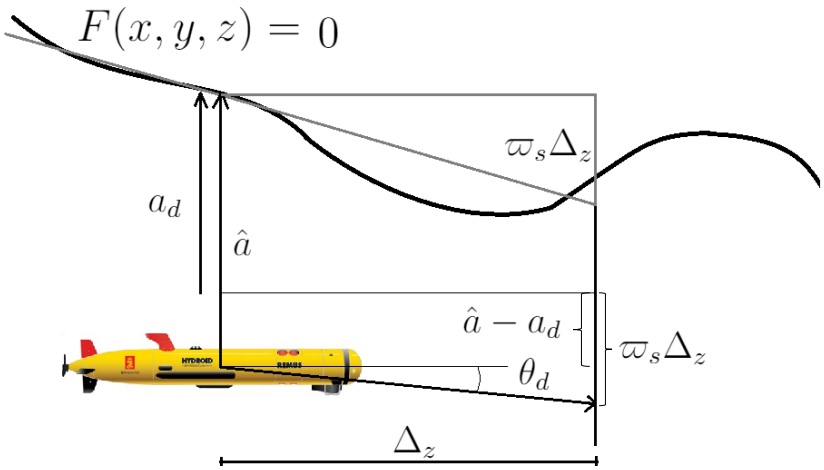

Figure 7: Altitude LOS guidance law with $k_{dive} = k_{ascent} = 1.0$.

The steering law in (50) may be interpreted as a saturating proportional feedback controller with a feedforward term:

$$\theta_d = \arctan\left(k_p(a - a_d) + v_{ff}\right) \tag{51}$$

where $k_p = 1/\Delta_z$ is the proportional gain, and $v_{ff} = \varpi_s$ is the feedforward term. The feedforward term will ensure that the vehicle responds instantly to changes in the ice surface slope.

The main advantages of the feedforward term is that it improves the tracking performance and it reacts instantly to changes in the ice surface slope. By using upwards-looking DVL with angles inclined slightly forwards, some collision avoidance properties are also obtained, as it will react instantly to changes in the ice surface slope in front of the vehicle.

A block diagram of the altitude observer and guidance system is shown in Figure 8.

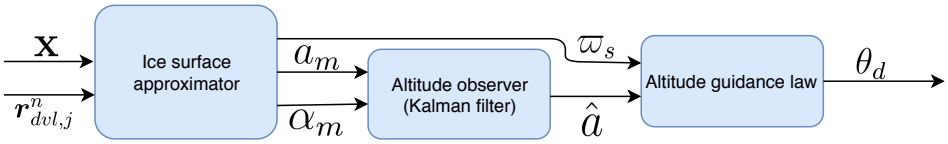

Figure 8: Block diagram of altitude observer and guidance system

2.7 Modeling of hybrid dynamical systems

Most often, a dynamical system is characterized as either a continuous-time system or a discrete-time system. Some systems, however, exhibit characteristics that are typical of both continuous-time systems and discrete-time systems. We call these hybrid systems. Some examples of hybrid systems are given in [26]. For more extensive details regarding the hybrid system framework, the reader is referred to [20].

2.7.1 The modeling framework

The hybrid dynamical system framework presented in [20] use a combination of differential inclusions to describe the continuous-time dynamics, referred to as flow, and difference inclusions to describe the discrete-time events, referred to as jumps. A general mathematical model of a hybrid system using this framework is given by

$$\mathcal{H} = \begin{cases} \boldsymbol{x} \in C & \dot{\boldsymbol{x}} \in \boldsymbol{F}(\boldsymbol{x}) \\ \boldsymbol{x} \in D & \boldsymbol{x}^+ \in \boldsymbol{G}(\boldsymbol{x}) \end{cases} \tag{52}$$

where $\boldsymbol{x}$ is the hybrid state, $C \subset \mathbb{R}^n$ is the flow set, $\boldsymbol{F} : \mathbb{R}^n \rightrightarrows \mathbb{R}^n$ is the flow map, $D \subset \mathbb{R}^n$ is the jump set and $\boldsymbol{G} : \mathbb{R}^n \times \mathbb{R}^m \rightrightarrows \mathbb{R}^n$ is the jump map. When the hybrid state $\boldsymbol{x}$ is in the flow set C, the system will flow according to the differential inclusion $\boldsymbol{F}(\boldsymbol{x})$, and when the hybrid state $\boldsymbol{x}$ is in the jump set D, the system will jump according to the difference inclusion $\boldsymbol{G}(\boldsymbol{x})$.

The advantage of this framework is that it allows modeling and stability analysis of many types of hybrid systems, e.g. systems with logic variables, mechanical systems with impacts, and computer sampled systems.

2.7.2 Example: Sample-and-hold control

To illustrate this framework of hybrid system modeling, we give an example of sample-and-hold control [20].

Given a continuous-time state-feedback controller, a sample-and-hold implementation of the feedback control law consists of two steps: i) *sample*: measure the state of the system, and use the feedback control law to compute the control signal, and ii) *hold*: apply the computed constant control signal for a certain amount of time. This procedure is then repeated indefinitely. Suppose that the plant is given by

$$\dot{\boldsymbol{z}} = \tilde{\boldsymbol{f}}(\boldsymbol{z}, \boldsymbol{u}) \tag{53}$$

where $\boldsymbol{z} \in \mathbb{R}^{n_p}$ is the state of the plant, $\boldsymbol{u} \in \mathbb{R}^{n_c}$ is the control variable and $\tilde{\boldsymbol{f}} : \mathbb{R}^{n_p} \times \mathbb{R}^{n_c} \to \mathbb{R}^{n_p}$ is the function describing the dynamics of the plant. Let $\boldsymbol{u} = \boldsymbol{\kappa}(\boldsymbol{z})$ be the state-feedback control law.

In order to implement this as a sample-and-hold strategy, we model the system using the hybrid system framework. In this model, the flow represents the continuous-time dynamics of the plant, and the jumps represent the sampling update process. We define the hybrid state variable

$$\boldsymbol{x} = \begin{bmatrix} \boldsymbol{z} \\ \boldsymbol{u} \\ \tau \end{bmatrix} \in \mathbb{R}^{n_p+n_c+1}. \tag{54}$$

where τ i a timer variable keeping track of the flow time. Let T denote the sampling time of the sample-and-hold control strategy, such that flow occurs when τ belongs to the interval $[0, T)$. During flow, the state of the plant $\boldsymbol{z}$ evolves according to the dynamics in (53), the control variable $\boldsymbol{u}$ is held constant, and τ keeps track of the elapsed time. Thus, the flow set and flow map may be given as

$$C = \mathbb{R}^{n_p} \times \mathbb{R}^{n_c} \times [0, T), \qquad \boldsymbol{f}(\boldsymbol{x}) = \begin{bmatrix} \tilde{\boldsymbol{f}}(\boldsymbol{z}, \boldsymbol{u}) \\ 0 \\ 1 \end{bmatrix}. \tag{55}$$

During a jump, the state of the plant remains unchanged, the control variable is updated according to the state-feedback control law $\boldsymbol{u} = \boldsymbol{\kappa}(\boldsymbol{z})$ and the timer τ is reset to zero. Jumps occur when τ reaches T. The jump set and jump map may then be formulated as

$$D = \mathbb{R}^{n_p} \times \mathbb{R}^{n_c} \times T, \qquad \boldsymbol{g}(x) = \begin{bmatrix} \boldsymbol{z} \\ \boldsymbol{\kappa}(\boldsymbol{z}) \\ 0 \end{bmatrix}. \tag{56}$$

2.8 Probabilistic reasoning and decision-making over time

Agents operating in the real world need to handle uncertainty due to partial observability and non-determinism in the environment. An agent at a given time does not know for certain its states, or where it will end up after a sequence of actions.

The most common tool for dealing with uncertainty is probability theory. Probability provides a way of summarizing the uncertainty that comes from theoretical and practical ignorance and incompetence in modeling the environment. This section presents background theory on probabilistic reasoning and decision-making.

2.8.1 Bayesian networks

A Bayesian network is a probabilistic graphical model that represents a set of variables and their conditional dependencies in the form of a directed acyclic graph, where each node is annotated with quantitative probability information. The syntax of Bayesian networks is defined as follows:

1. A set of chance nodes representing random and uncertain variables.
2. A set of arcs representing direct influence between a pair of nodes, forming a directed acyclic graph. If there is an arc from node X to node Y, X is said to be the parent of Y, and Y the child of X.
3. A conditional probability distribution $\boldsymbol{P}(X_i|Parents(X_i))$ quantifying the influence of the parents on each node.

The *global semantics* of Bayesian networks defines the full joint distribution as the product of the local conditional distributions. A joint distribution is the probability of a conjunction of particular assignments to each variable $P(X_1 = x_1 \wedge ... \wedge X_n = x_n)$, shortened $P(x_1, ..., x_n)$. A specific joint distribution is given by the formula

$$P(x_1, ..., x_n) = \prod_{i=1}^{n} P(x_i | parents(X_i)), \tag{57}$$

where $parents(X_i)$ denotes the values of the parents of the variable X_i that appear in $x_1, ..., x_n$.

The *local semantics* of Bayesian networks specifies that: i) a node is conditionally independent of its non-descendants given its parents, and ii) a node is conditionally independent of all other nodes in the network given its Markov blanket - that is, its parents, children and childrens' parents.

Inference in a Bayesian network refers to the computation of the posterior probability distribution for a set of query variables, given some event - that is, some assignment of values for a set of observable variables. There exist algorithms for both exact and approximate inference. Typical methods for exact inference are inference by enumeration and the variable elimination algorithm. For large, multiply connected networks where exact inference is intractable, approximate inference methods are used. Typical methods for approximate inference includes randomized sampling algorithms, also called Monte Carlo algorithms.

2.8.2 Dynamic Bayesian networks

A dynamic Bayesian network is a Bayesian network that represents a temporal probability model [8]. They can be seen as a generalization of hidden Markov chains and Kalman filters. A simple dynamic Bayesian network for two-dimensional robot navigation with battery monitoring is shown in Figure 9.
The four main inference tasks for dynamic Bayesian networks are *filtering*, *prediction*, *smoothing* and *most likely explanation*:

Filtering: The task of computing the posterior distribution over the most recent state, given all evidence to data - that is, computing $\boldsymbol{P}(\boldsymbol{X_t}|\boldsymbol{e}_{1:t})$.

Prediction: The task of computing the posterior distribution over a future state, given all evidence to data - that is, computing $\boldsymbol{P}(\boldsymbol{X_{t+k}}|\boldsymbol{e}_{1:t})$ for some $k > 0$.

Smoothing: The task of computing the posterior distribution a past state, given all evidence to data - that is, computing $\boldsymbol{P}(\boldsymbol{X_k}|\boldsymbol{e}_{1:t})$ for some k such that $0 \leq k < t$.

Most likely explanation: The task of computing the most likely sequence of states to have generated a set of observations - that is, computing $\text{argmax}_{\boldsymbol{x}_{1:t}} P(\boldsymbol{x}_{1:t}|\boldsymbol{e}_{1:t})$.

2.8.3 Bayesian networks for risk modeling

Bayesian networks have been used for risk assessments in various domains, e.g. prediction of risk of vehicle loss of AUVs during their missions [27], autonomous subsea intervention

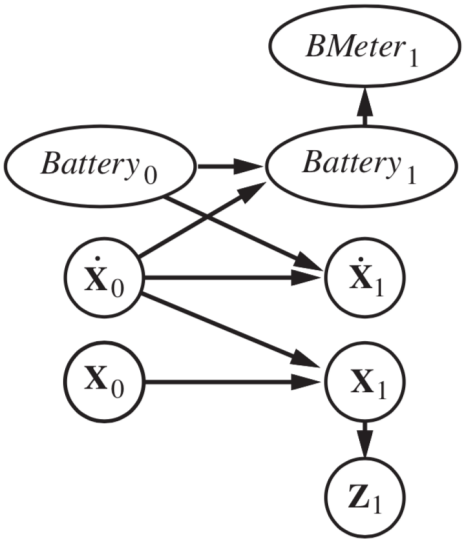

Figure 9: Simple dynamic Bayesian network for two-dimensional robot navigation with two time steps. Here the position, velocity and battery are not directly observable, but noisy measurements of position and battery are available. Image courtesy of [8].

operations [28] and risk assessment of human-autonomy collaboration for autonomous marine systems.

We propose a generic structure for modeling risk with Bayesian networks. In this model, we define a root node for risk of an accidental event with two parents, namely the probability of that event occuring and the consequence(s) of that event. The root node may, if wished, be replaced with a utility node, supporting different kinds of definitions of risk, e.g. probability times consequence. Also, a series of these trees may be connected to a new root node when including multiple accidental events. Figure 10 shows the generic Bayesian network structure following this idea.

Dynamic Bayesian networks may be useful for autonomous decision-making when taking the temporal aspect of risk into consideration. Filtering may be used to improve the current risk estimate by incorporating more evidence. Prediction is particularly useful for mission planning, as the predicted future evolution of risk may be taken into account when replanning the mission. Smoothing is important for learning, as it provides better estimates of past states than was available at the time by incorporating more evidence.

2.8.4 Decision networks

Decision networks are graphical representations of a system involving a decision [8]. Decision networks are created by extending a Bayesian network to also include *decision nodes* and *utility nodes*. Decision nodes represent points where the agent has a choice of actions, whereas utility nodes represent the agent's utility function. The utility nodes' parents are all variables describing the outcome state that directly affects the utility. This may provide a substrate for implementing utility-based AUV agents, as introduced in section 1.2.1.

In decision networks, actions are traditionally selected by evaluating the decision network for each possible setting of the decision nodes, and choosing the decisions yielding the

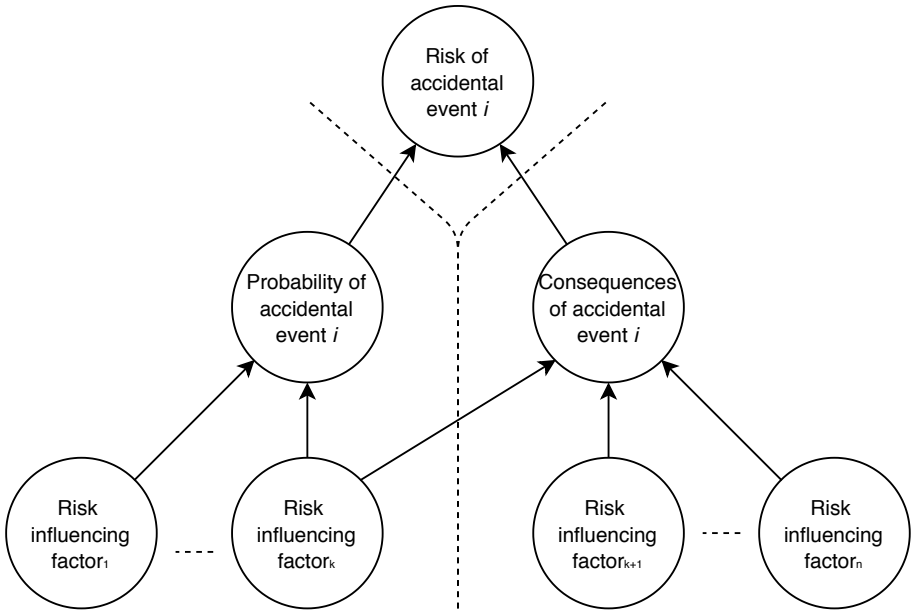

Figure 10: Generic structure of Bayesian network for calculating the risk of a hazardous event. Note that one risk influencing factor may influence both the probability and the consequence(s) of an accidental event.

highest expected utility. This is often called the principle of maximum expected utility (MEU). After an action for a decision node has been set, it behaves like a chance node with acquired evidence. The algorithm for for choosing an action given a decision network by unconstrained maximization of utility is as follows [8]:

1. Set the evidence variables for the current state.
2. For each possible value of the decision node:
   (a) Set the decision node to that value.
   (b) Calculate the posterior probabilities for the parent nodes of the utility node, using a standard probabilistic inference algorithm.
   (c) Calculate the resulting utility for the action.
3. Return the action giving the highest utility.

2.8.5 Markov decision processes

Most decision problems are sequential by nature, where the agent's utility depends on a sequence of decisions. Sequential decision problems incorporate utilities, uncertainty and sensory information, and include search and planning problems as special cases [8].

A Markov decision process (MDP) is a mathematical framework for modeling a sequential decision problem for a fully observable, stochastic environment with additive rewards and a Markovian transition model - that is, the probability of reaching a new state s' depends only on the current state s, and not on the previous history of states. Formally, an MDP is represented by the tuple $(\mathcal{S}, \mathcal{A}, \mathcal{T}, \mathcal{R})$, where:

- $\mathcal{S}$ is a set of states $\{s_1, ..., s_n\}$,

- $\mathcal{A}$ is a set of actions $\{a_1, ..., a_n\}$,
- $\mathcal{T} : \mathcal{S} \times \mathcal{A} \times \mathcal{S} \rightarrow [0, 1]$ is a transition function that represents conditional transition probabilities between states s and s' when executing action a - that is, $\mathcal{T}(s, a, s') = P(s'|a, s)$,
- $\mathcal{R} : \mathcal{S} \times \mathcal{A} \rightarrow \mathbb{R}$ is a reward function.

The solution of an MDP is a policy $\pi(s)$ - that is, the recommended action by the policy π for state s. Due to the stochastic nature of the environment, executing a given policy starting from an initial state s_0 may lead to a different history of states. An optimal policy $\pi^*(s)$ is therefore a policy that yields the highest expected utility. The expected utility obtained by executing a policy π starting in state s when using discounted utilities with infinite horizons is given by

$$U^{\pi}(s) = E\left[\sum_{t=0}^{\infty} \gamma^t \mathcal{R}(S_t)\right] \tag{58}$$

where S_t is a random variable denoting the state the agent reaches at time t when performing some policy π. The optimal policy is found from solving

$$\pi^*(s) = \text{argmax}_{a \in \mathcal{A}(s)} \sum_{s} P(s'|a, s)U(s'). \tag{59}$$

The true utility of a state is then given by $U^{\pi^*}(s)$, and is the expected sum of discounted rewards if the agents executes an optimal policy π^* starting in s. The value iteration algorithm and policy iteration algorithm may be used for iteratively calculating an optimal policy.

2.8.6 Partially observable Markov decision processes

A partially observable Markov decision process (POMDP) is an MDP with a partially observable environment; the agent does not know for sure which state it is in. Therefore, it does not make sense to talk about a state-dependent policy $\pi(s)$. As the underlying state is not directly observable, the agent instead maintains a probability distribution over all possible state based on a set of observations and observation probabilities, namely a belief state b. Formally, a POMDP is represented by the tuple $(\mathcal{S}, \mathcal{A}, \mathcal{T}, \mathcal{R}, \mathcal{Z}, \mathcal{O})$, where:

- $\mathcal{S}$ is a set of states $\{s_1, ..., s_n\}$,
- $\mathcal{A}$ is a set of actions $\{a_1, ..., a_n\}$,
- $\mathcal{T} : \mathcal{S} \times \mathcal{A} \times \mathcal{S} \rightarrow [0, 1]$ is a transition function that represents conditional transition probabilities between states s and s' when executing action a - that is, $\mathcal{T}(s, a, s') = P(s'|a, s)$,
- $\mathcal{R} : \mathcal{S} \times \mathcal{A} \rightarrow \mathbb{R}$ is a reward function,
- $\mathcal{Z}$ is a set of observations $\{e_1, ..., e_n\}$,
- $\mathcal{O} : \mathcal{S} \times \mathcal{Z} \rightarrow [0, 1]$ is a sensor function that represents conditional observation probabilities between observation e and state s - that is, $\mathcal{O}(e, s) = P(e|s)$.

A belief state summarizes all relevant infomation in the observation, and is updated as new observations are made. A new belief state $b'(s')$ is updated according to

$$b'(s') = \alpha P(e|s') \sum_{s} P(s'|a, s)b(s) \tag{60}$$

where $b(s)$ is the previous belief state, and α is a normalizing constant that makes the probability distribution of the belief state sum to 1. This is essentially the filtering task as described in 2.8.2.

The solution of a POMDP is an optimal policy $\pi^*(b)$ mapping belief states to actions. An optimal policy over an infinite horizon can be found by maximizing the expected cumulative discounted reward R_t at time t with discount factor γ, when executing π starting from the initial belief state b_0,

$$\pi^* = \text{argmax}_\pi E\left[\sum_{t=0}^{\infty} \gamma^t \mathcal{R}(S_t)|b_0\right]. \tag{61}$$

One way of solving POMDPs is by conversion to an MDP in the continuous belief-state space and using either a value iteration or a policy iteration algorithm. Large POMDPs may be solved by approximation using Monte Carlo tree search.

2.8.7 Chance-constrained POMDPs

Agents operating in partially observable stochastic environments often face the problem of optimizing the expected cumulative discounted reward while bounding the probability of violating safety constraints. Such problems may be modeled as chance-constrained POMDPs (CC-POMDP). The objective of a CC-POMDP is to find an optimal policy π^* according to

$$\pi^* = \text{argmax}_\pi E\left[\sum_{t=0}^{\infty} \gamma^t \mathcal{R}(S_t)|b_0\right], \text{ s.t. } P\left(\bigvee_{t=1}^{n} S_t \notin \mathcal{C}\right) \leq \delta \tag{62}$$

where $\mathcal{C} \subseteq \mathcal{S}$ is a set of safe states and δ is a bound on the probability of some event happening during policy execution. The RAO* algorithm, a heuristic forward search algorithm, may be used to obtain optimal, deterministic, finite-horizon policies for CC-POMDPs [29].

2.8.8 Application of POMDPs for Arctic operations of AUVs

Ocean processes are subject to large spatial and temporal variability, and often, it is not possible to examine the examine entire environment in detail [30]. The lack of sufficient observations is the largest source of error in our understanding. This is the sampling problem of oceanography [31]. Also, due to poor knowledge about the environment beneath the Arctic sea ice, offline planning prior to the mission may be inefficient with respect to data gathering. This forms the motivation for development of information-driven sampling strategies in Arctic operations of AUVs. Through online intelligent decision-making based on in-situ sensory information, allows sampling efforts to be concentrated to regions with high scentific interest, but at the same time, take into account the associated risks.

Recent studies have shown that Markovian approaches show promise for the application of information-driven sampling, taking into account uncertainty in the environment. This may prove to be relevant for improving the robustness, as well as the effeciency, of Arctic operations of AUVs in ocean research applications. Below follow some applications of Markovian approaches in online planning of mobile agents:

- In [32], sequential Bayesian optimization is used within a POMDP (BO-POMDP) for environment monitoring with UAVs. Here, the pose of the agent is assumed fully observable, whereas the studied phenomenon is described by a (partially observable) Gaussian process (GP).

- In [33] considers time-varying MDPs (TVMDP), decision problems in which the environment varies in both space and time. This framework is able to adapt to future time-varying transition dynamics over some horizon. They examplify with a marine robotics motion planning application, where the discrete MDP state space is converted to a continuous state space.

- In [34], measurement maximizing adaptive sampling is framed as a chance-constrained MDP (CC-MDP) with a risk bounding function. Here, a mobile agent with uncertain position taking measurements in a Gaussian process with known mean and covariance kernel is tasked with maximizing the expected sum of future measurements while bounding the probability it collides with the environment.

Using the framework of CC-POMDPs, one may model the temporal probability of vehicle loss under the sea ice using dynamic Bayesian networks, and constrain this probability with a bound. Further, one may use sequential Bayesian optimization for adaptive sampling of phenomena modeled by GP in Arctic oceans, and make decisions by solving for an optimal policy in the CC-POMDP online. This is topic for future research.

3 Simulator setup and validation

In this chapter, details regarding the case study, simulation environment and setup are presented.

3.1 Hybrid observer simulation

In the first appended paper, a hybrid observer concept was implemented and simulated in MATLAB/Simulink using the Hybrid Equations Toolbox v2.04 [35]. This toolbox was developed for simulation of hybrid dynamical systems as described in section 2.7.

3.2 Arctic AUV simulator

The simulator environment used in this thesis is an Arctic AUV simulator created by Norgren [19] in MATLAB/Simulink and C++. This simulator was created mainly for testing AUV guidance systems for iceberg detection and iceberg mapping using simultaneous localization and mapping (SLAM). The simulated DVL beam ranges in conjunction with the AUV dynamics have been implemented by Holsen in [36], and further developed by Norgren [19]. The Bayesian network risk model was implemented in Simulink with C++ using the `dlib` package [37].

The vehicle dynamics implemented in the simulator is based on the REMUS-100 AUV, following the mathematical models presented in chapter 2. The numerical values for the mathematical model can be found in Appendix A. An image of the REMUS-100 AUV is showed in Figure 11.

Figure 11: REMUS-100 AUV. Image courtesy of Kongsberg Maritime [38].

3.3 Ice data

In the simulator, three-dimensional floe-scale map of sea-ice drafts compiled from expiditions by an AUV to the near-coastal regions of the Weddel, Bellingshausen and Wilkes Land sectors of Antarctica, developed by Williams et al. [39] and [40], was used. The compiled ice data was modified such that it was compatible by the Arctic AUV simulator described in section 3.2.

4 Conclusions

In this thesis, tools and methods for developing robust autonomy of underwater vehicles in Arctic operations have been evaluated. This chapter summarizes the major findings and contributions of the two appended papers, presents recommendations for further work and concludes this thesis.

4.1 Concluding remarks

The main conclusions of the appended papers are summarized as follows:

Paper 1: A method for the design of a six DOF sensor-based hybrid translational observer is proposed, accounting for noisy, asynchronous and sporadically available sensor measurements. High-frequency noise it filtered out by taking a weighted discounted average of a finite number of previous measurements predicted forwards to the current time. It is successfully able to estimate the states, filter out high-frequency noise, and showed robustness in terms of larger maximum update rates and acceleration measurement noise. The performance depended on the number of observer states and the values of the discount factors. The values of these parameters should be tuned according to the relative uncertainty in the measurements governing the jump dynamics and the flow dynamics.

Paper 2: A method for intelligent risk-based under-ice altitude control for AUVs is presented. An altitude guidance law for following a contour of the ice surface using DVL measurements is proposed, where a desired pitch angle is computed based on the estimated altitude error and the estimated slope of the ice surface in the vehicle heading direction. Furthermore, a method for online probabilistic reasoning over the current state of risk using Bayesian networks for AUVs operating under ice is developed. The model captures the probability of vehicle loss through a susceptibility node, and the consequences of vehicle loss through a recovery ineffectiveness node, which together constitute the risk of vehicle loss. The network is then extended to a decision network for autonomously selecting the setpoint for the altitude controller yielding the highest reward while subject to a constraint on the risk. Simulations shows that the AUV successfully follows a contour of the ice undersurace, and adapts to the varying level of risk throughout its mission by reselecting the altitude setpoint.

The framework of hybrid dynamical systems seems promising for the design and analysis of navigational systems for autonomous vehicles. It is able to handle the continuous nature of predictions and the discrete nature of sampling updates, with noisy, asynchronous and sporadically available sensor measurements, in a unified framework. It also allows for rigorous mathematical stability analysis. In order to implement intelligent control, situation awareness and decision-making capabilities for improved robustness and safety of autonomous systems, integrating methods from the control theory with methods from the AI community, such as Bayesian and Markovian approaches, seems promising.

4.2 Suggestions for further work

During the course of this work, a number of interesting topics for further studies have been identified. The following issues are recommended for further studies:

Paper 1: The performance of the proposed sensor-based hybrid observer concept should be evaluated in closed-loop with a feedback controller, an attitude observer, a gravity model and a guidance scheme. Rigorous stability analysis using the stability theory of hybrid systems and cascaded systems should be done for more formal proofs of stability. Establishing certain recurrence properties of the observer when including stochastic effects of noise in the position and velocity measurements are also of interest.

Paper 2: A thorough comparison of the proposed altitude guidance law with and without the feedforward on the estimated slope of the ice surface is of interest. A more extensive Bayesian network risk model should be developed. Extending the network to a dynamic Bayesian network, allowing for prediction of the future evolution of risk if also of interest. Also, the risk-bound in paper 2 was static. A topic for future research is to include a dynamic risk-bound. The risk-bound may e.g. be a function of the reward, such that higher rewards justifies accepting higher risks, or be a function of the uncertainty in the estimates, such that more uncertain risk estimates are accommodated with more conservative risk-bounds.

Other: By using a dynamic risk model in the form of a dynamic Bayesian network, the frameworks of chance-constrained MDPs/POMDPs seem promising for calculating optimal policies while constraining the probability of entering unsafe states. Using a Markovian approach, uncertainty in the environment and the future evolution of states is incorporated in the decision-making. These frameworks are also compatible with sequential Bayesian optimization over a Gaussian process, with applications such as risk-constrained adaptive robotic sampling.

References

[1] National Snow and Ice Data Center. *Freezing in the Dark*. http://nsidc.org/arcticseaicenews/2017/11/freezing-in-the-dark/. [Online; accessed 10-October-2018]. 2018.

[2] G.T. Farmer and J. Cook. *Climate change science: A modern synthesis: Volume 1 - The physical climate*. Springer Netherlands, 2013, pp. 1–564. ISBN: 9789400757578.

[3] Kwang-Yul Kim et al. "Mechanism of seasonal Arctic sea ice evolution and Arctic amplification". In: *The Cryosphere* 10.5 (2016). ISSN: 1994-0416.

[4] Sandra Connelly. "Ice Albedo Feedback". In: *Encyclopedia of Global Warming Climate Change* (2012), pp. 744–745.

[5] Jørgen Berge et al. "Unexpected Levels of Biological Activity during the Polar Night Offer New Perspectives on a Warming Arctic". In: *Current Biology* 25.19 (2015), pp. 2555–2561. DOI: 10.1016/j.cub.2015.08.024. URL: http://dx.doi.org/10.1016/j.cub.2015.08.024.

[6] U.S. State Department. *Freezing in the Dark*. http://www.state.gov/e/oes/ocns/opa/arc/uschair/258202.htm. [Online; accessed 10-October-2018]. 2014.

[7] Martin Ludvigsen and Asgeir J. Sørensen. "Towards integrated autonomous underwater operations for ocean mapping and monitoring". In: *Annual Reviews in Control* 42 (2016), pp. 145–157. ISSN: 1367-5788.

[8] Stuart Russell and Peter Norvig. *Artificial Intelligence: A Modern Approach*. 3rd. Upper Saddle River, NJ, USA: Prentice Hall Press, 2009. ISBN: 0136042597, 9780136042594.

[9] Committee on Autonomous Vehicles in Support of Naval Operations. *Autonomous vehicles in support of naval operations*. Washington, D.C.: National Research Council (U.S.). Committee on Autonomous Vehicles in Support of Naval Operations, 2005.

[10] Mae L. Seto. *Marine Robot Autonomy*. 2013th ed. Vol. 9781461456599. Springer Verlag, 2013. ISBN: 1461456584.

[11] Ingrid B. Utne Asgeir J. Sørensen and Ingrid Schjølberg. "Risk Management of Autonomous Marine Systems and Operations". In: *ASME 2017 36th International Conference on Ocean, Offshore and Arctic Engineering* 3.B (2017).

[12] *Autonomous vehicles in support of naval operations*. National Academies Press, 2005, pp. 1–238. ISBN: 0309096766.

[13] Cambridge Dictionary. *Definition of robustness*. https://dictionary.cambridge.org/dictionary/english/robustness. [Online; accessed 11-Juner-2019].

[14] Tristan Perez, Alejandro Donaire, and Brendan P. Willams. "On Evaluation of Robust Autonomy for Uninhabited Vehicles and Systems". eng. In: *IFAC Proceedings Volumes* 43.16 (2010), pp. 348–353. ISSN: 1474-6670.

[15] Stan Franklin. "An Agent Architecture Potentially Capable of Robust Autonomy". In: (Jan. 2001).

[16] David Kortenkamp. "The Roles of Machine Learning in Robust Autonomous Systems". In: 2001.

[17] Woods Hole Oceanographic Institution. *Images: Communicating Under Sea Ice*. https://www.whoi.edu/oceanus/v2/article/images.do?id=248951. [Online; accessed 11-November-2018]. 2018.

[18] Stanley Kaplan and B. John Garrick. "On The Quantitative Definition of Risk". In: *Risk Analysis* 1.1 (), pp. 11–27. DOI: 10.1111/j.1539-6924.1981.tb01350.x. eprint: https://onlinelibrary.wiley.com/doi/pdf/10.1111/j.1539-6924.1981.tb01350.x. URL: https://onlinelibrary.wiley.com/doi/abs/10.1111/j.1539-6924.1981.tb01350.x.

[19] Petter Norgren. "Autonomous underwater vehicles in Arctic marine operations : Arctic marine research and ice monitoring". In: Doktoravhandlinger ved NTNU (trykt utg.) 2018:255 (2018).

[20] Rafal Goebel. *Hybrid Dynamical Systems : Modeling, Stability, and Robustness*. eng. Princeton, 2012.

[21] Fredrik Dukan and Asgeir J. Sørensen. "Sea floor geometry approximation and altitude control of ROVs". In: *Control Engineering Practice* 29 (2014), pp. 135–146. ISSN: 0967-0661.

[22] Thor I. Fossen. *Handbook of Marine Craft Hydrodynamics and Motion Control*. Chichester, UK: John Wiley Sons, Ltd, 2011. ISBN: 9781119991496.

[23] John Carlton. *Marine Propellers and Propulsion*. 2nd ed. Elsevier Science, 2007. ISBN: 0750681500.

[24] Timothy Prestero. *Development of a Six-Degree of Freedom Simulation Model for the REMUS Autonomous Underwater Vehicle*. Tech. rep. 2002. URL: http://handle.dtic.mil/100.2/ADA409034.

[25] Environment and Climate Change Canada. *Ice Glossory*. https://www.ec.gc.ca/glaces-ice/default.asp?lang=En&n=501D72C1-1&def=hide1B6894C57. [Online; accessed 14-November-2018]. 2018.

[26] Michael Stephen Branicky. *Studies in hybrid systems : modeling, analysis, and control*. eng. Cambridge, Mass, 1995.

[27] Mario Brito and Gwyn Griffiths. "A Bayesian approach for predicting risk of autonomous underwater vehicle loss during their missions". In: *Reliability Engineering System Safety* 146 (2016), pp. 55–67. ISSN: 0951-8320. DOI: https://doi.org/10.1016/j.ress.2015.10.004. URL: http://www.sciencedirect.com/science/article/pii/S0951832015002860.

[28] Jeevith Hegde et al. "A Bayesian approach to risk modeling of autonomous subsea intervention operations". eng. In: *Reliability Engineering System Safety* 175 (2018). ISSN: 0951-8320. URL: http://search.proquest.com/docview/2073130157/.

[29] Pedro Santana, Sylvie Thiébaux, and Brian Williams. "RAO*: An Algorithm for Chance-constrained POMDP's". In: *Proceedings of the Thirtieth AAAI Conference on Artificial Intelligence*. AAAI'16. Phoenix, Arizona: AAAI Press, 2016, pp. 3308–3314. URL: http://dl.acm.org/citation.cfm?id=3016100.3016366.

[30] Trygve Olav Fossum et al. "Information-driven robotic sampling in the coastal ocean". In: *Journal of Field Robotics* 35.7 (2018), pp. 1101–1121. ISSN: 1556-4959.

[31] R.H. Stewart. *Introduction to Physical Oceanography*. University Press of Florida, 2009. ISBN: 9781616100452. URL: https://books.google.no/books?id=3dXTRAAACAAJ.

[32] Philippe Morere, Roman Marchant, and Fabio Ramos. "Sequential Bayesian Optimisation as a POMDP for Environment Monitoring with UAVs". In: (2017).

[33] Lantao Liu and Gaurav S. Sukhatme. "A Solution to Time-Varying Markov Decision Processes". In: (2016).

[34] B. Ayton, B. Williams, and R Camilli. "[TO BE PUBLISHED]]". In: 2019.

[35] Ricardo G. Sanfelice, David A. Copp, and Pablo Nanez. "A toolbox for simulation of hybrid systems in matlab/simulink: hybrid equations (HyEQ) toolbox". In: *HSCC*. 2013.

[36] Sigurd Andreas Holsen. *DUNE: Unified Navigation Environment for the REMUS 100 AUV - Implementation, Simulator Development, and Field Experiments*. 2015. URL: http://hdl.handle.net/11250/2350792.

[37] Davis E. King. "Dlib-ml: A Machine Learning Toolkit". In: *Journal of Machine Learning Research* 10 (2009), pp. 1755–1758.

[38] Kongsberg Maritime. *Autonomous underwater vehicle, REMUS 100*. https://www.kongsberg.com/maritime/products/marine-robotics/autonomous-underwater-vehicles/AUV-remus-100/. [Online; accessed 25-June-2019]. 2019.

[39] Guy D. Williams et al. "Beyond Point Measurements: Sea Ice Floes Characterized in 3-D". In: *Eos, Transactions American Geophysical Union* 94.7 (2013), pp. 69–70. ISSN: 0096-3941.

[40] G Williams et al. "Thick and deformed Antarctic sea ice mapped with autonomous underwater vehicles". eng. In: *Nature Geoscience* 8.1 (2015), pp. 61–67. ISSN: 17520894. URL: http://search.proquest.com/docview/1657287407/.

[41] B. Allen, W.S. Vorus, and T. Prestero. "Propulsion system performance enhancements on REMUS AUVs". In: vol. 3. IEEE Publishing, 2000, pp. 1869–1873. ISBN: 0780365518.

Paper 1

Sensor-Based Hybrid Translational Observer For Underwater Navigation

Jens E. Bremnes, Astrid H. Brodtkorb, Asgeir J. Sørensen

Accepted and to be published at the 12th IFAC Conference on Control Applications in Marine Systems (CAMS2019),
Daejeon, Korea

Sensor-Based Hybrid Translational Observer For Underwater Navigation

Jens E. Bremnes * **Astrid H. Brodtkorb** * **Asgeir J. Sørensen** *

* *Centre for Autonomous Marine Operations and Systems (AMOS), Department of Marine Technology, Norwegian University of Science and Technology (NTNU), Otto Nielsens veg 10, 7491 Trondheim, Norway (e-mails: jens.e.bremnes@ntnu.no, astrid.h.brodtkorb@ntnu.no, asgeir.sorensen@ntnu).*

Abstract: Accurate underwater navigation systems are required for closed-loop guidance and control of unmanned underwater vehicles (UUV). This paper proposes a method for the design of a six degrees-of-freedom (DOF) sensor-based hybrid translational observer concept for underwater navigation using the hybrid dynamical systems framework, accounting for noisy, asynchronous and sporadically available sensor measurements. Sensor measurements from an acoustic positioning system, a Doppler Velocity Log (DVL), an Inertial Measurement Unit (IMU) and a pressure gauge are used in the proposed observer. A method for filtering high-frequency noise is proposed, where the estimated states are obtained by taking a weighted discounted average of a finite number of previous measurements predicted forwards to the current time. The attitude of the vehicle is assumed known, and acceleration measurements are assumed to be continuously available. Measurements of position, depth and linear velocity are assumed to be available sporadically with asynchronous sampling rates. Results from simulations are presented to demonstrate the performance of the proposed method.

Keywords: Hybrid dynamical systems, observers, underwater navigation

1. INTRODUCTION

Accurate underwater navigation systems are required for closed-loop guidance and control of UUVs. Most UUVs today use model-based observers. By including a kinetic model of the vehicle, these observers are able to filter out noise, reconstruct unmeasured states, estimate biases, and in the case of signal loss, do dead reckoning. Steinke and Buckham (2005) propose a Kalman filter for Remotely Operated Vehicles (ROV). Drawbacks of Kalman filters are the large number of parameters to be tuned, and the unproved mathematical stability proofs for certain applications. On the contrary, nonlinear passive filters are able to provide proof of global stability. Refsnes et al. (2007) propose a nonlinear passive observer for UUVs. A shortcoming of model-based observers is that the bias estimate is not able to capture rapidly changing loads and environmental conditions, making them perform poorly during transients.

Sensor-based observers on the other hand, often called a strap-down approach, rely purely on the sensor measurements and kinematic relationships. Thus, all unknown forces acting on the vehicle are captured in the observer instantaneously by the accelerometers. In Dukan (2014) a sensor-based integration filter for the estimation of translational motion of UUVs is proposed. A drawback of strap-down approaches is that these solutions are sensitive to the accuracy of the attitude estimation, and, in the case of signal loss, are not able to predict the states in a satisfying manner. A good model of the gravity and centripetal accelerations is also required.

Most approaches to observer design assume that sensor measurements are continuously available, or that the sampling rates remain constant. In Brodtkorb et al. (2016), a 3 DOF observer combining measurements of different fidelities for estimation of translational motion for marine vessels is proposed. However, here it is assumed that both the position and velocity measurements are obtained together at a non-constant sampling rate.

The main contribution of this paper includes the development of a method for the design of a 6 DOF sensor-based translational observer using the framework of hybrid dynamical systems proposed by Goebel et al. (2012) applied to UUVs, accounting for noisy, asynchronous and sporadically available sensor measurements. The attitude of the UUV is assumed known, and the acceleration measurements are assumed to be continuously available. The observer is modeled as a cascaded system of three hybrid observers, where acceleration measurements and velocity estimates are continuously integrated in order to obtain velocity and position predictions, corrected by occasional discrete measurement updates. Each hybrid observer keeps a finite number of the most recent measurements, predicted forward to the current time using the flow dynamics. A method for filtering high-frequency measurement noise

⋆ This work was supported by the Research Council of Norway through the Centre of Excellence funding scheme, NTNU AMOS, project number 90311502, and the UNLOCK project, through the Research Council of Norway FRINATEK scheme, project number 223254.

is proposed, where the position and velocity estimates are obtained by taking a weighted discounted average of the observer states, giving higher trust to more recent predictions. Results from simulations presented to demonstrate the performance of the proposed methods. Robustness with respect to acceleration measurement noise and increased sampling time is also evaluated.

The paper is organized as follows: In Section 2, the kinematic equations of the observer is presented, as well as the hybrid dynamical systems framework. The observer design is proposed in Section 3. The observer is tested in simulations using MATLAB/Simulink in Section 4. Section 5 concludes the paper.

2. MATHEMATICAL MODELING

2.1 Kinematics of an underwater vehicle

The 6 DOF equation of motion for an underwater vehicle is expressed by the Earth-fixed position vector $\boldsymbol{\eta} = [\boldsymbol{p}\ \boldsymbol{\Theta}]^T = [N\ E\ D\ \phi\ \theta\ \psi]^T \in \mathbb{R}^6$ and the body-fixed velocity vector $\boldsymbol{\nu} = [\boldsymbol{v}\ \boldsymbol{\omega}]^T = [u\ v\ w\ p\ q\ r]^T \in \mathbb{R}^6$, where the three first elements in the vectors correspond to the linear part of the motion, and the three latter elements correspond to the angular part of the motion. The signal-based translational observer is based on the kinematic relationship between the Earth-fixed linear velocities $\dot{\boldsymbol{p}}$ and the body-fixed linear velocities $\boldsymbol{v}$ through the transformation

$$\dot{\boldsymbol{p}} = \boldsymbol{R}_b^n(\boldsymbol{\Theta})\boldsymbol{v} \tag{1}$$

where $\boldsymbol{R}_b^n(\boldsymbol{\Theta})$ denotes the Euler angle transformation given by

$$\boldsymbol{R}_b^n(\boldsymbol{\Theta}) = \begin{bmatrix} c\psi c\theta & -s\psi c\phi + c\psi s\theta s\phi & s\psi s\phi + c\psi c\theta s\phi \\ s\psi c\theta & c\psi c\phi + s\phi s\theta s\psi & -c\psi s\phi + s\theta s\psi c\phi \\ -s\theta & c\theta s\phi & c\theta c\phi \end{bmatrix}$$

and $s\cdot = \sin(\cdot)$, $c\cdot = \cos(\cdot)$ and $t\cdot = \tan(\cdot)$.

2.2 Hybrid Dynamical Systems

The hybrid dynamical system framework presented in Goebel et al. (2012) can be used to model and analyze systems with both continuous and discrete dynamics. In general, this can be modeled as

$$\mathcal{H} = \begin{cases} \boldsymbol{x} \in C & \dot{\boldsymbol{x}} \in \boldsymbol{F}(\boldsymbol{x}) \\ \boldsymbol{x} \in D & \boldsymbol{x}^+ \in \boldsymbol{G}(\boldsymbol{x}) \end{cases} \tag{2}$$

where $C \subset \mathbb{R}^n$ is the flow set, $\boldsymbol{F} : \mathbb{R}^n \rightrightarrows \mathbb{R}^n$ is the flow map, $D \subset \mathbb{R}^n$ is the jump set and $\boldsymbol{G} : \mathbb{R}^n \times \mathbb{R}^m \rightrightarrows \mathbb{R}^n$ is the jump map.

2.3 Measurements

UUVs typically navigate using four different sensors: inertial measurement units (IMU), Doppler Velocity Logs (DVL), pressure gauges and hydroacoustic transponders (Ludvigsen and Sørensen, 2016). IMUs combine accelerometers for linear acceleration measurements and gyroscopes for angular velocity measurements, DVLs are used to measure linear velocities, pressure gauges measure depth, and transponders, part of an acoustic positioning system, measure position relative to a transducer. These measurements are taken at different sampling rates, ranging from $100 - 200$ Hz for IMU linear acceleration and angular velocity measurements, $0.5 - 5$ Hz for DVL linear velocity measurements, $0.8 - 8$ Hz for pressure gauges depth measurements, and $0.1 - 2$ Hz for acoustic positioning measurements.

It is assumed that the position, depth and velocity measurements are obtained with a non-constant sample time in the interval $[\underline{T}_j, \bar{T}_j]$ with Gaussian distributed noise with variance σ_j^2 for $j \in \{1, 2, 3\}$, where the index $j = 1$ represents acoustic positioning measurements, $j = 2$ represents pressure gauge depth measurements, and $j = 3$ represents DVL velocity measurements.

In the design of the observer, it is assumed that the measured acceleration $\boldsymbol{a}$ is equal to the real acceleration of the vehicle - that is, the measurements do not contain any noise or biases. However, in the numerical simulations, noise is included. Also, it is assumed that the vehicle's attitude $\boldsymbol{\Theta}$ is known.

3. HYBRID OBSERVER DESIGN

A method for the design of a cascaded sensor-based hybrid translational observer $\mathcal{H}$ consisting of a hybrid sub-system $\mathcal{H}_3$ in cascade with two other hybrid sub-systems $\mathcal{H}_1$ and $\mathcal{H}_2$, where $\mathcal{H}_3$ is a velocity observer, $\mathcal{H}_1$ is a position observer, and $\mathcal{H}_2$ is a depth observer, is proposed. A block diagram of the cascaded hybrid observer structure is shown in Figure 1.

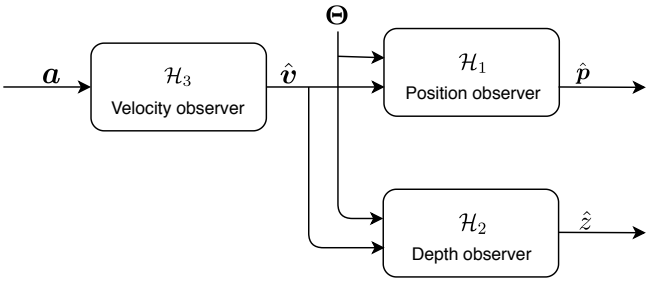

Fig. 1. Block diagram showing the cascade structure of the hybrid observer.

Each observer has N_j observer states, denoted $(\cdot)_i$ for $i \in \{1, ..., N_j\}$, $j \in \{1, 2, 3\}$, representing copies of position, depth and velocity measurements predicted forwards to the current time using the flow dynamics by integration. The observer states work as a first-in-first-out (FIFO) queue. New measurements are stored in the first observer state $(\cdot)_1$, while the remainder of the states are shifted one place back. The last observer state $(\cdot)_{N_j}$ with the most outdated prediction is pushed out of the queue and deleted. The time before a new measurement is randomly selected from an interval $[\underline{T}_j, \bar{T}_j]$, where $\underline{T}_j$ and $\bar{T}_j$ represent the lower and upper bound for the sampling time characterized by sensor j, respectively.

For filtering high-frequency noise, a method inspired by a weighting scheme in Sørensen (2013) is proposed. The observer estimates are obtained by taking a weighted discounted average of the observer states, given by

$$\hat{\boldsymbol{p}} := \frac{\sum_{i=1}^{N_1} \gamma_1^i \boldsymbol{p}_i}{\sum_{i=1}^{N_1} \gamma_1^i}, \quad \hat{z} := \frac{\sum_{i=1}^{N_2} \gamma_2^i z_i}{\sum_{i=1}^{N_2} \gamma_2^i}, \quad \hat{\boldsymbol{v}} := \frac{\sum_{i=1}^{N_3} \gamma_3^i \boldsymbol{v}_i}{\sum_{i=1}^{N_3} \gamma_3^i} \tag{3}$$

where $\gamma_j \in (0,1]$, $j \in \{1,2,3\}$, is a constant discount factor. The motivation for using a weighted discounted average is that we have a higher trust in more recent predictions, as these states have integrated possible errors for a shorter time. Note that when $\gamma_j = 1$, we get the mean value of the observer states. In Figure 2, an example of a time series of the evolution of the observer states in the position observer with $N_1 = 3$ is shown. A large variance and a constant sampling rate of $T_3 = 5$ seconds on the position measurement was included for better visualization. The observer is initialized at the true position.

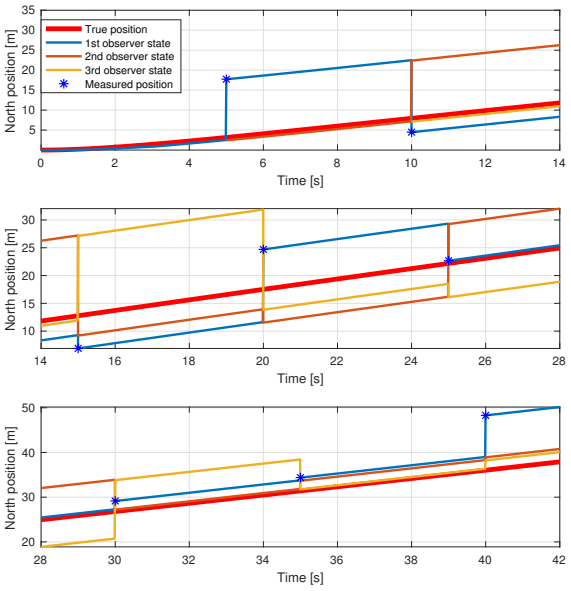

Fig. 2. Time series of the evolution of the position observer states with $N_1 = 3$. The estimated position at a given time is found by taking the weighted discounted average of the three observer states.

In the velocity observer $\mathcal{H}_3$, the dynamics flow with the acceleration measurements in between the velocity measurements - that is, when $\tau_3 \in [0, \bar{T}_3]$. The observer states are then updated discretely when new velocity measurements are available. The counter variable τ_3 counts backwards in time, such that jumps are triggered when $\tau_3 = 0$. The velocity observer is, for $i \in \{1, ..., N_3\}$, given by

$$\mathcal{H}_3 := \begin{cases} \left.\begin{aligned} \dot{\boldsymbol{v}}_i &= \boldsymbol{a} \\ \dot{\tau}_3 &= -1 \end{aligned}\right\} & (\boldsymbol{v}_i, \tau_3) \in \mathbb{R}^3 \times [0, \bar{T}_3] \\ \left.\begin{aligned} \boldsymbol{v}_i^+ &= \boldsymbol{v}_{i-1} \\ \tau_3^+ &\in [\underline{T}_3, \bar{T}_3] \end{aligned}\right\} & (\boldsymbol{v}_i, \tau_3) \in \mathbb{R}^3 \times \{0\} \end{cases} \tag{4}$$

where $\boldsymbol{v}_0 = \boldsymbol{v}$ is the DVL linear velocity measurement.

In the position observer $\mathcal{H}_1$, the position states flow with the velocity estimate in (3), and are similarly updated discretely when new position measurements are available. The position observer is, for $i \in \{1, ..., N_1\}$, given by

$$\mathcal{H}_1 := \begin{cases} \left.\begin{aligned} \dot{\boldsymbol{p}}_i &= \begin{bmatrix} 1 & 0 & 0 \\ 0 & 1 & 0 \end{bmatrix} \boldsymbol{R}_b^n(\boldsymbol{\Theta}) \hat{\boldsymbol{v}} \\ \dot{\tau}_1 &= -1 \end{aligned}\right\} & (\boldsymbol{p}_i, \tau_1) \in \mathbb{R}^2 \times [0, \bar{T}_1] \\ \left.\begin{aligned} \boldsymbol{p}_i^+ &= \boldsymbol{p}_{i-1} \\ \tau_1^+ &\in [\underline{T}_1, \bar{T}_1] \end{aligned}\right\} & (\boldsymbol{p}_i, \tau_1) \in \mathbb{R}^2 \times \{0\} \end{cases} \tag{5}$$

where $\boldsymbol{p}_0 = \boldsymbol{p}$ is the acoustic position measurement.

The vertical position is measured by a pressure gauge, as it provides higher accuracy and sampling rate than the acoustic positioning system. Therefore, we utilize these measurements for the depth estimate, encapsulated by the depth observer $\mathcal{H}_2$, for $i \in \{1, ..., N_2\}$:

$$\mathcal{H}_2 := \begin{cases} \left.\begin{aligned} \dot{z}_i &= \begin{bmatrix} 0 & 0 & 1 \end{bmatrix} \boldsymbol{R}_b^n(\boldsymbol{\Theta}) \hat{\boldsymbol{v}} \\ \dot{\tau}_2 &= -1 \end{aligned}\right\} & (z_i, \tau_1) \in \mathbb{R} \times [0, \bar{T}_2] \\ \left.\begin{aligned} z_i^+ &= z_{i-1} \\ \tau_2^+ &\in [\underline{T}_2, \bar{T}_2] \end{aligned}\right\} & (z_i, \tau_2) \in \mathbb{R} \times \{0\} \end{cases} \tag{6}$$

where $z_0 = z$ is the pressure gauge depth measurement.

4. SIMULATION RESULTS AND DISCUSSION

This Section presents the setup of the simulations, and discusses the results.

4.1 Setup

The observer was implemented in MATLAB/Simulink using the Hybrid Equations Toolbox v2.04 (Sanfelice et al., 2013). Open-loop zig-zag motions in the horizontal plane and yo-yo motions in the vertical plane with zero sway and heave velocities were simulated, while the surge velocity is accelerated from 0 to 1 meters per second. This gives an indicator of the observer performance, however, the performance may be different in closed-loop with a feedback control system, an attitude observer and a gravity model. The simulated motion of the vehicle is for simplicity and without loss of generality prescribed and given by

$$\begin{aligned} \theta(t) &= 0.4 \sin(0.05t) \\ \psi(t) &= 0.03 \sin(0.2t) \\ u(t) &= 1 - \exp(-0.5t) \end{aligned}$$

The initial conditions of the UUV are zero for all states, except for an initial depth of 50 m.

The observer is simulated for different values of the number of observer states N_1, N_2 and N_3, the discount factors γ_1, γ_2 and γ_3, maximum sampling time $\bar{T}_1$, $\bar{T}_2$ and $\bar{T}_3$, and different levels of noise σ_{imu} on the acceleration measurements. All observer states are initialized at zero, not at the current state of the vehicle.

For the sake of order, a reference simulation case is established. All other simulations are small perturbations on one of the parameters of the reference simulation case. The numerical values of the reference simulation cases are given below in Table 1.

		Observer type		
		Position ($j=1$)	Depth ($j=2$)	Velocity ($j=3$)
N_j	[-]	10	10	10
γ_j	[-]	0.85	0.85	0.85
$\underline{T}_j$	[s]	0.5	0.125	0.2
$\bar{T}_j$	[s]	10	1.250	2.0

Table 1. Numerical values for the reference simulation case.

Measurement noise with standard deviations $\sigma_{imu} = 0.007$ $[m/s^2]$, $\sigma_1 = 0.5$ $[m]$, $\sigma_2 = 0.001$ $[m]$ and $\sigma_3 = 0.003$ $[m/s]$ were added on the IMU, acoustic positioning system, pressure gauge and DVL measurements, respectively.

4.2 Simulation results and discussions

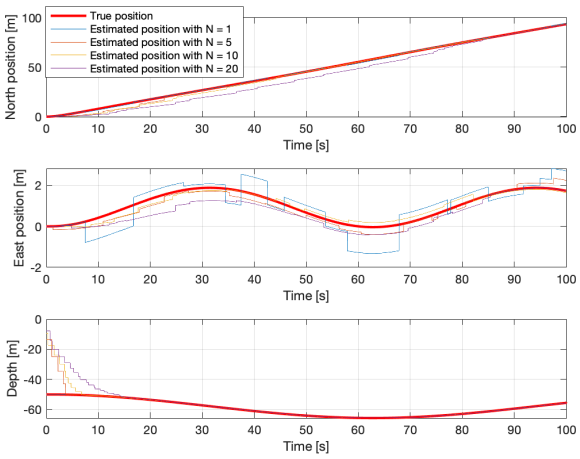

Fig. 3. Position observer performance for different number of observer states N_1, N_2 and N_3.

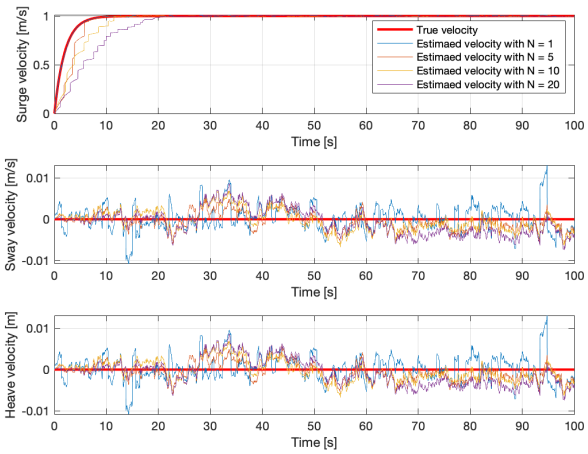

Fig. 4. Velocity observer performance for different number of observer states N_1, N_2 and N_3.

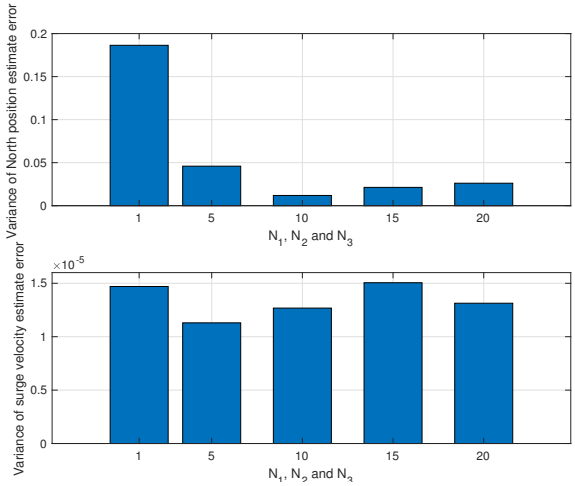

Fig. 5. Stationary variance of the North position and surge velocity estimate error for different values of N_1, N_2 and N_3.

Figures 3-4 show the estimated positions and velocities for different numbers of observer states N_1, N_2 and N_3. In general, we see that the variance of the estimate decreases with increasing number of states. However this also increases the transient time. In Figure 5, where the corresponding stationary variance of the North position and surge velocity estimate errors is shown, we see that the variance of the position error estimates decrease by increasing the number of states in the observer up to a certain point, before it increases again. The rapid decrease in variance for low values of N_1, N_2 and N_3 is due to the high variance of the position measurements. However, when the number of states is too large, the estimates are to a larger extent based on older predictions where possible errors have been integrated for a longer time. The same trend is not so obvious for the surge velocity estimate error variance. This is due to the low uncertainty in the velocity measurements, in contrast to the high uncertainties in the acoustic position measurements. The results will also suffer from random effects differing from simulation to simulation.

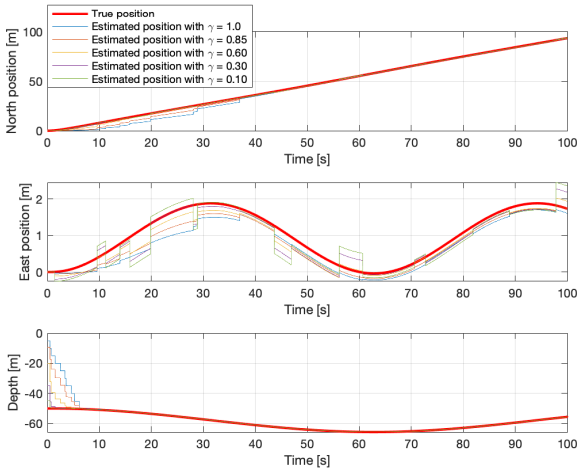

Fig. 6. Position observer performance for different values of the discount factors γ_1, γ_2 and γ_3.

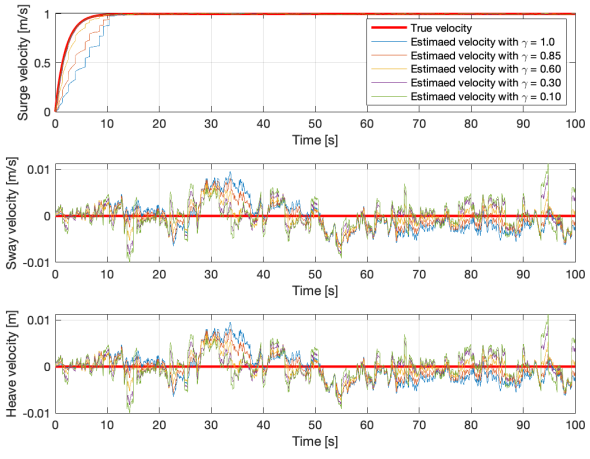

Fig. 7. Velocity observer performance for different values of the discount factors γ_1, γ_2 and γ_3.

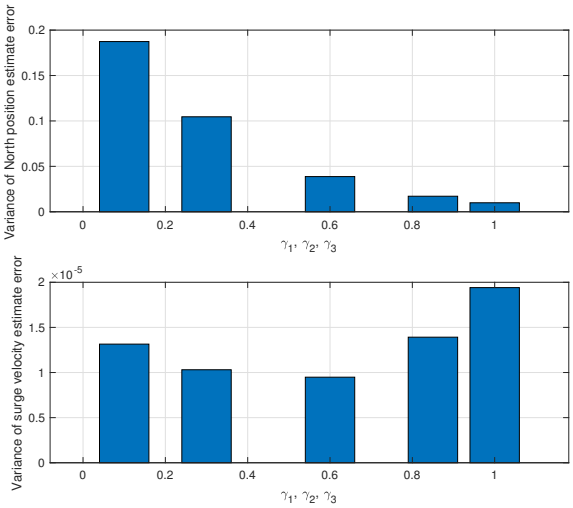

Fig. 8. Stationary variance on the North position and surge velocity estimate error for different values of the discount factors.

Figures 6-7 show the observer estimates for different values of the discount factors γ_1, γ_2 and γ_3. The corresponding stationary variance of the North position and surge velocity error estimate is shown in Figure 8. As can be seen, decreasing the discount factor increases the variance of the position estimate errors. This is due to the high uncertainty in the position measurements; lower values of the discount factor results in neglect of the older predictions, thus reducing its noise mitigation properties. For the velocity estimates, however, reducing the discount factor reduces the variance of the velocity estimate errors up to a certain point, before it is increased again. This is because the velocity measurements have low uncertainty relative to the uncertainty introduced by integration of acceleration noise.

There seems to be optimal values for the number of observer states and the discount factors with respect to position and velocity estimation error variance. These values should be chosen with basis in the relative uncertainty in the measurements governing the jump dynamics and the flow dynamics.

Figures 9-10 show the performance of the observer with increased values of the maximum sampling time; the sampling time is increased by a factor ranging up to 10. As seen, the observer is quite robust in terms of slow update rates. Figure 11 shows the stationary variance of the North position and the surge velocity estimate for the same results. As seen, the estimation error variance seems to grow exponentially with increased sampling periods. The position estimate is particularly sensitive to increased sampling times.

Figures 12-13 show the performance of the observer for different levels of acceleration measurement noise. As can be seen, the performance is alao quite robust with respect to acceleration measurement noise. It is not until the noise is in the order of 30 the normative value that the estimated states get considerably noisy. Figure 14 shows the corresponding stationary estimation error variance.

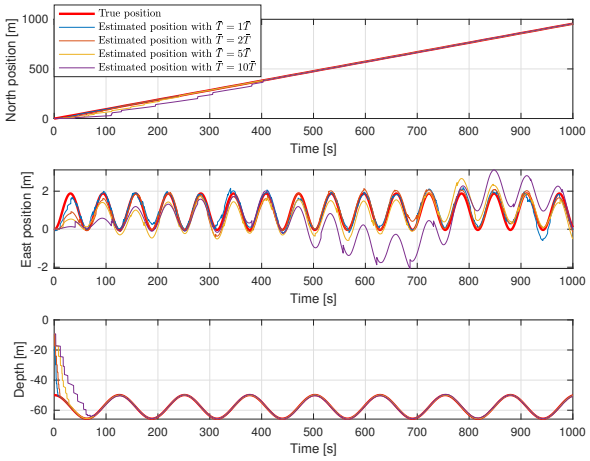

Fig. 9. Position observer performance with different values of the maximum sampling rates.

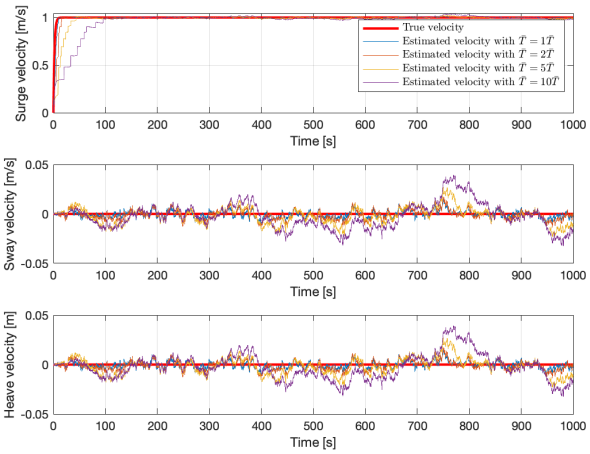

Fig. 10. Velocity observer performance with different values of the maximum sampling rates.

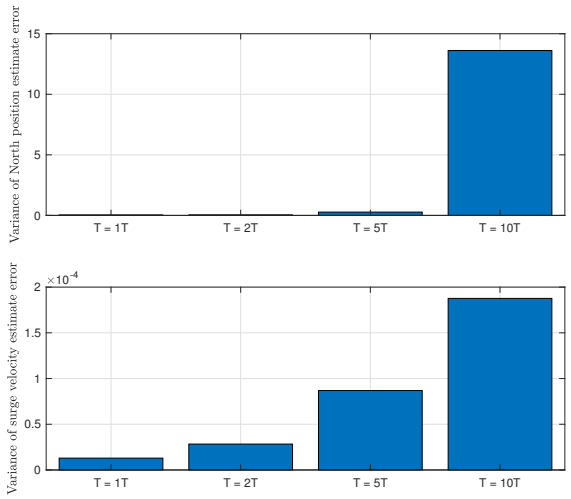

Fig. 11. Stationary variance of the North position and surge velocity estimate error for different values of the maximum sampling time.

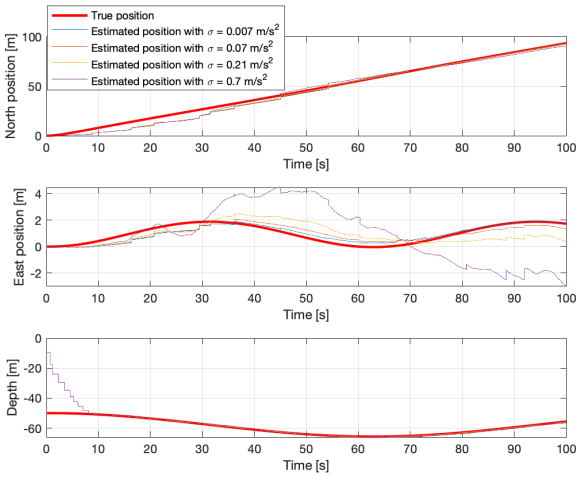

Fig. 12. Position observer performance for different levels of the acceleration measurement noise.

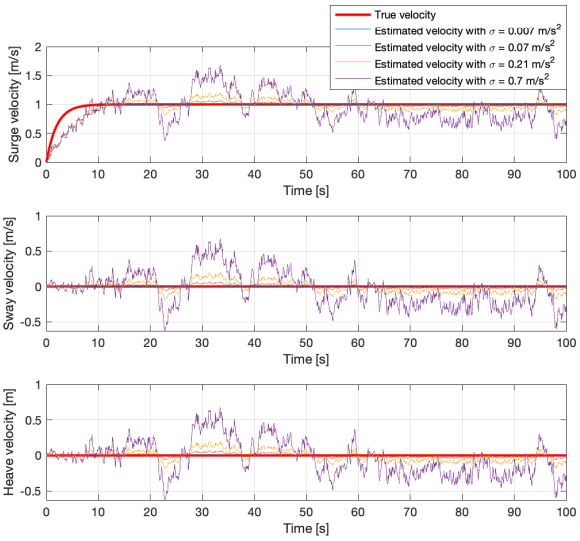

Fig. 13. Velocity observer performance for different levels of the acceleration measurement noise.

It should be noted that the estimated state is discontinuous during jumps; after each measurement update, the estimate will experience a jump. When using the estimated states in a feedback control system, the estimated state trajectory should be smooth. It will therefore be necessary to filter out the discontinuities using e.g. a low-pass filter.

For future work, the observer performance should be evaluated in closed-loop with a feedback controller, an attitude observer, a gravity model and a guidance scheme. Due to the cascaded structure, errors in the velocity estimate output from the velocity observer $\mathcal{H}_3$ will affect the estimates of the position observer $\mathcal{H}_1$ and the depth observer $\mathcal{H}_2$. Rigorous stability analyses using stability theory of hybrid systems and cascaded systems, providing more formal proofs of stability, is needed. Also, establishing certain robustness and recurrence properties when taking into account the effect of noise in the measurements, as well as errors in the attitude estimation, is of interest.

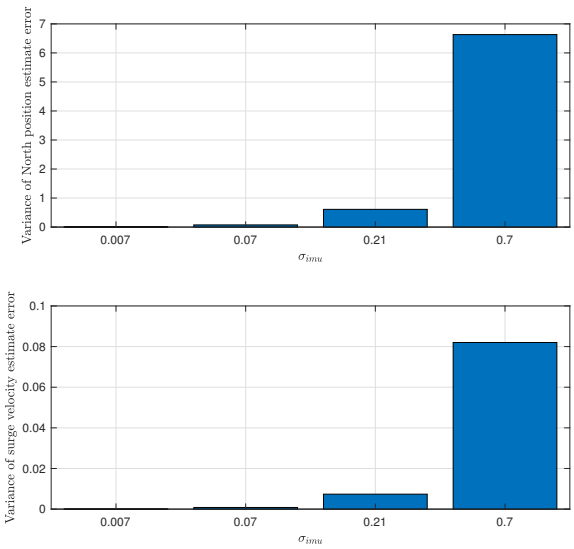

Fig. 14. Stationary variance of the North position and surge velocity estimate error for different levels of acceleration measurement noise.

5. CONCLUSIONS

The proposed sensor-based hybrid translational observer performed well in the simulations. The performance depended on the number of states N_1, N_2 and N_3 in the observers and the discount factors γ_1, γ_2 and γ_3. The value of these parameters should be tuned according to the relative uncertainty in the measurements governing the jump dynamics and the flow dynamics. The observer also showed robustness in terms of larger values of the maximum update rates $\bar{T}_1$, $\bar{T}_2$ and $\bar{T}_3$ and the acceleration measurement noise.

REFERENCES

Brodtkorb, A.H., Teel, A.R., and Sørensen, A.J. (2016). Hybrid observer combining measurements of different fidelities. *IFAC PapersOnLine*, 49(23), 506–511.

Dukan, F. (2014). ROV motion control systems.

Goebel, R., Salfelice, R.G., and Teel, A.R. (2012). Hybrid dynamical systems : Modeling, stability, and robustness.

Ludvigsen, M. and Sørensen, A.J. (2016). Towards integrated autonomous underwater operations for ocean mapping and monitoring. *Annual Reviews in Control*, 42, 145–157.

Refsnes, J., Sørensen, A.J., and Pettersen, K.Y. (2007). A 6 dof nonlinear observer for AUVs with experimental results. In *2007 Mediterranean Conference on Control Automation*, 1–7. doi:10.1109/MED.2007.4433891.

Sanfelice, R.G., Copp, D.A., and Nanez, P. (2013). A toolbox for simulation of hybrid systems in matlab/simulink: hybrid equations (hyeq) toolbox. In *HSCC*.

Sørensen, A.J. (2013). Marine control systems : Propulsion and motion control of ships and ocean structures.

Steinke, D. and Buckham, B. (2005). A kalman filter for the navigation of remotely operated vehicles. In *Proceedings of OCEANS 2005 MTS/IEEE*, volume 2005, 581–588 Vol. 1. IEEE.

Paper 2

Intelligent Risk-Based Under-Ice Altitude Control for Autonomous Underwater Vehicles

Jens E. Bremnes, Petter Norgren, Asgeir J. Sørensen,

Christoph A. Thieme, Ingrid B. Utne

Draft paper under review at the OCEANS 2019 Seattle Conference.
Seattle, The United States of America

Intelligent Risk-Based Under-Ice Altitude Control for Autonomous Underwater Vehicles

Jens E. Bremnes*, Petter Norgren*, Asgeir J. Sørensen*, Christoph A. Thieme*, Ingrid B. Utne*

*Centre for Autonomous Marine Operations and Systems (AMOS),
Department of Marine Technology, Norwegian University of Science and Technology (NTNU),
NO-7491 Trondheim, Norway.
{jens.e.bremnes, petter.norgren, asgeir.sorensen, christoph.thieme, ingrid.b.utne}@ntnu.no

***Abstract*—Autonomous underwater vehicles (AUVs) are effective platforms for mapping and monitoring under the sea ice in polar oceans. However, under-ice operations impose demanding requirements to the system, as it must deal with uncertain and unstructured environments, harsh environmental conditions and reduced capabilities of navigational sensors. This paper presents a method for intelligent risk-based under-ice altitude control for AUVs. Firstly, an altitude guidance law for following a contour of the ice surface via pitch control using measurements from a Doppler velocity log (DVL) is proposed. Furthermore, a Bayesian network for probabilistic reasoning over the current state of risk during the operation is developed. This network is then extended to a decision network for autonomous risk-based selection and reselection of the setpoint for the altitude controller, balancing the trade-off between the reward of the setpoint and the risk involved. This will improve the system safety and reliability during under-ice operations. Results from a simulation study is presented in order to demonstrate the performance of the proposed method.**

***Index Terms*—underwater robotics, guidance, control, Bayesian networks, decision-making, risk modeling, probabilistic reasoning, artificial intelligence**

I. Introduction

Intelligent autonomous vehicles composed of advanced control, decision and sensor systems are emerging, and are essential for allowing new and challenging operations, such as mapping and monitoring of the oceans, inspections and interventions of structures difficult to access, and autonomous transportation, both land based and at sea. As the level of autonomy in systems increase, and the missions become more complex, stricter requirements related to safe system performance are imposed. The vehicle must be able to navigate through unknown and unstructured environments, handle unforeseen hazardous situations and faults, and make informed decisions.

Autonomous underwater vehicles (AUVs) are effective platforms for ocean research and monitoring. However, as operations of AUVs move towards challenging environments such as under sea ice, under shelf ice or along rocky coasts, the risk increases. AUV operations at Arctic latitudes and under the ice are complicated by harsh environmental conditions, uncertain and unstructured ice environments and reduced capabilities of navigation sensors. For example, Australian and British AUVs have been lost under ice sheets [1]. Therefore, increased situational awareness and decision-making capabilities are required for safe system performance. One of the tools for achieving this is online risk management through intelligent risk-based control, reasoning and decision-making.

Risk management is constituted by risk assessment, monitoring, control and follow-up of risk [2]. Utne et al. [3] clarify, categorize and classify risk related to autonomous marine systems, and establish a foundation for risk management of such systems. They discuss that risk management should become a driver in the design and operation of highly automated intelligent systems. An autonomous system should be able to determine if it can continue with possible degraded performance, assess the level of tolerable risk by improving situational awareness capabilities, and carry out decisions based on perception, comprehension and projection of the future situation that we today leave to a human operator [3].

Brito and Griffiths [4] and [5] use Bayesian networks to predict risk of vehicle loss of AUVs during their missions, including under the sea ice. Their approach was more focused on offline prediction prior to the mission.

Optical mapping closer to the ice surface is often considered more scientifically rewarding due to the existance of algae and phytoplankton and other biological phenomena here. However, this is also associated with higher risks. There is therefore a balance between the reward of flying closer to the surface, and the risk involved in doing so. The main contribution of this paper is a method for intelligent risk-based under-ice altitude control. The altitude under the ice is controlled to an altitude setpoint via pitch control. A risk model in the form of a Bayesian network is developed for online reasoning over the current state of risk, ranging from low to high risk, during operation. Using sensor data, evidential reasoning is used for online update of the posterior probability distribution of the current state of risk. This information is then used for autonomously selecting and reselecting the altitude setpoint, and whether or not to abort the mission.

The paper is organized as follows: In Section 2, background theory on risk, Bayesian networks and decision networks is described. Section 3 presents the methods for altitude estimation

This work was supported by the Research Council of Norway through the Centre of Excellence funding scheme, NTNU AMOS, project number 90311502, and the UNLOCK project, through the Research Council of Norway FRINATEK scheme, project number 223254.

and under-ice altitude control. Section 4 describes the method for developing the Bayesian network risk model. In Section 5, the network is extended to a decision network for autonomous risk-based decision-making. Simulation results and discussions are given in Section 6. Section 7 concludes this paper and presents the scope for future work.

II. Risk modeling using Bayesian networks

This section presents background theory on risk, probabilistic modeling using Bayesian networks, and how this may be extended to a decision problem using decision networks.

A. Definition of risk

In [6], the risk related to an hazardous event e_i may be represented by a triplet

$$r = \{e_i, c_i, q\}|k \tag{1}$$

where c_i is the consequence(s) of e_i, q is a measure of the uncertainty involved, and k is the background knowledge used for determining e_i, c_i and q. For autonomous systems operating in an unstructured environment, with little or no apriori information, q may be assumed to be high and k low [3]. We adopt this definition in this paper.

B. Risk management of AUVs

According to Utne et al. [3], risk control of autonomous systems can occur in two, complementary ways: i) risk control *of* the autonomous system, mostly relevant for systems with low levels of autonomy, and ii) risk control *by* the autonomous system, mostly relevant for systems with high levels of autonomy. In this paper, we consider risk control done by the system itself.

C. Bayesian networks

Bayesian networks have been used for risk assessments in various domains.

Bayesian networks are directed acyclic graphs where nodes represent uncertain variables, and the arcs represent direct causal dependencies between a child node and a parent node. Each node has a conditional probability table (CPT) that determines the probability distribution of a child's states based on the parents' states. In most available Bayesian network software tools, the embedded inference algorithms can support four types of reasoning: predictive, diagnostic, combined and intercausal reasoning [7]. Predictive reasoning algorithms may be applied to the network to calculate the posterior probability distributions of uncertain variables based on new evidence. Such predictions may be factual, e.g. based on new evidence, or hypothetical, e.g. predicting the effect of an intervention.

A Bayesian network is typically composed of target nodes, intermediate nodes and observable nodes. Target nodes are the nodes in which the joint probability distributions are to be calculated. Intermediate nodes are mainly defined to help manage the size of the CPTs, as well as making the model more transparent. The observable nodes represent variables that are measurable or directly observable.

Bayesian networks presents a natural framework for situational awareness, information fusion and human-like reasoning for autonomous systems. It provides the systems with the ability to interpret situations based on incomplete and uncertain information, detect abnormal behaviours and patterns, self-diagnosis and performance monitoring, which in turn may support the system in online decision-making.

For underwater robotics, Bayesian networks have been applied for risk modeling of, for example, vehicle loss during their missions [4], human-autonomy collaboration [8] and subsea intervention operations [9]. Some other common risk modeling frameworks, such as fault trees, may be mapped into a Bayesian network.

D. Decision networks

Decision networks, also called influence diagrams, combine Bayesian networks with additional node types for decisions and utilities [10]. Chance nodes represent the random variables, i.e. the nodes that constitute the Bayesian networks. Decision nodes represents points where the decision maker has a choice of actions. Utility nodes represents the decision maker's utility as function of the parent attributes.

III. Altitude estimation and control

In this case study, we want the AUV to follow a contour of the ice surface, which is achieved by altitude control. We consider an AUV equipped with an upwards-looking DVL with four beams in a Janus configuration. This section presents a method for altitude estimation and pitch control for tracking the ice surface.

A. Kinematics

The position of the AUV in the Earth-fixed North-East-Down reference frame $\{n\}$ is $\boldsymbol{p} = [x, y, z]^T$. The velocity vector in $\{n\}$ is expressed as

$$\dot{\boldsymbol{p}} = \boldsymbol{R}_b^n(\boldsymbol{\Theta})\boldsymbol{v} \tag{2}$$

where $\boldsymbol{\Theta} = [\phi, \theta, \psi]$ is the attitude vector, $\boldsymbol{R}_b^n(\boldsymbol{\Theta})$ is the rotation matrix from the body-fixed reference frame $\{b\}$ to $\{n\}$, and $\boldsymbol{v} = [u, v, w]$ is the velocity vector in $\{b\}$ [11].

In the simplified case where the DVL is located at the center of origin of the AUV, the i^{th} DVL measurement can be expressed in $\{b\}$ as

$$\boldsymbol{r}_i^b = r_i \begin{bmatrix} \sin(\gamma_i)\cos(\beta_i) \\ \sin(\gamma_j)\sin(\beta_i) \\ -\cos(\gamma_i) \end{bmatrix} \tag{3}$$

where r_i is the i^{th} DVL beam range, and γ_i and β_i are the offset angles for the DVL beams along the vehicle's longitudinal and transversal direction, respectively. The i^{th} DVL measurement can then be expressed in $\{n\}$ from the rotation $\boldsymbol{r}_i^n = \boldsymbol{R}_b^n(\boldsymbol{\Theta})\boldsymbol{r}_i^b$.

B. Approximation of ice surface geometry, altitude and altitude rate

We define the altitude as the z component of the vector from the center of origin of the AUV to the point on the ice surface with the same horizontal coordinates expressed in $\{n\}$. Note that the altitude under the ice will be negative.

A method from Dukan et al. [12], originally developed for sea floor tracking, is used to approximate the geometry of the ice surface, the altitude and altitude rate of change.

We assume that the submerged ice surface in $\{n\}$ can be expressed by the equation

$$F(x, y, z) = f(x, y) - z = 0, \quad \frac{\partial F}{\partial t} = 0 \tag{4}$$

where F is a time-invariant function with continuous first-order partial derivatives. The altitude can then be written as

$$a = f(x, y) - z. \tag{5}$$

The altitude rate of change is found by differentiating (5) with respect to time

$$\dot{a} = \frac{\partial f}{\partial x}\frac{dx}{dt} + \frac{\partial f}{\partial y}\frac{dy}{dt} - \frac{dz}{dt}. \tag{6}$$

This may be rewritten as [12]

$$\begin{aligned} \dot{a} &= \nabla F(\boldsymbol{p})\dot{\boldsymbol{p}} \\ &= \left[\left.\frac{\partial f}{\partial x}\right|_{\boldsymbol{p}}, \left.\frac{\partial f}{\partial y}\right|_{\boldsymbol{p}}, -1\right] \boldsymbol{R}_b^n(\boldsymbol{\Theta}) \begin{bmatrix} u \\ v \\ w \end{bmatrix}. \end{aligned} \tag{7}$$

The ice surface is at each time step approximated as a linear surface $f(x, y) = a_m + bx + cy$ by using least squares regression utilizing all four DVL beams by solving

$$[a_m, b, c] = \text{argmin}_{a_m,b,c} \sum_{i=1}^{4} [a_i^n - (a_m + bx_i^n + cy_i^n)]^2. \tag{8}$$

The approximated altitude of the AUV is then a_m, and the corresponding approximated ice surface gradient vector is

$$\nabla \hat{F} = \left[\left.\frac{\partial \hat{f}}{\partial x}\right|_{\boldsymbol{p}}, \left.\frac{\partial \hat{f}}{\partial y}\right|_{\boldsymbol{p}}, -1\right] = [b,\ c,\ -1]. \tag{9}$$

The approximated altitude rate of change $\dot{a}_m$ is then given by

$$\dot{a}_m = \left[\left.\frac{\partial \hat{f}}{\partial x}\right|_{\boldsymbol{p}}, \left.\frac{\partial \hat{f}}{\partial y}\right|_{\boldsymbol{p}}, -1\right] \boldsymbol{R}_b^n(\hat{\boldsymbol{\Theta}}) \begin{bmatrix} \hat{u} \\ \hat{v} \\ \hat{w} \end{bmatrix} \tag{10}$$

where $\hat{(\cdot)}$ denotes an estimated value. In order to ensure a continuous and smooth estimate $\hat{a}$ of the altitude, a Kalman filter using the Euler integration method with state a_m and input $\dot{a}_m$ is used, see [12] for details. In this paper, we assume that the attitude and the velocity of the vehicle are known - that is, $\hat{\boldsymbol{\Theta}} = \boldsymbol{\Theta}$ and $\hat{\boldsymbol{v}} = \boldsymbol{v}$.

C. Altitude control

During altitude control, the control objective is to make the vehicle follow a contour of the ice surface while the horizontal trajectories are controlled independently. In this paper, we propose a line-of-sight (LOS) guidance law with lookahead-based steering in the vertical plane, where the vehicle pitch is controlled in order to obtain the desired altitude.

The slope of the ice surface in the vehicle heading direction may used to predict changes in the ice surface depth. This may be utilized in the altitude guidance law. The slope is approximated as

$$\varpi = \left.\frac{\partial \hat{f}_\psi}{\partial x}\right|_{\boldsymbol{p}} = [1, 0, 0]\boldsymbol{R}_{z,\psi}^{-1}(\hat{\psi}) \left[\left.\frac{\partial \hat{f}}{\partial x}\right|_{\boldsymbol{p}}, \left.\frac{\partial \hat{f}}{\partial y}\right|_{\boldsymbol{p}}, 0\right]^T \tag{11}$$

where $\boldsymbol{R}_{z,\psi}^{-1}(\hat{\psi})$ is the principal rotation matrix about the z axis from $\{n\}$ to $\{b\}$. Due to errors and noise in the estimation of ϖ, one might downscale it's effect in the guidance scheme. The downscaled ice surface slope used in the guidance law is given as

$$\varpi_s = [k_{dive}, k_{ascend}] \begin{bmatrix} \text{sat}^+(\varpi) \\ \text{sat}^-(\varpi) \end{bmatrix} \tag{12}$$

where $k_{dive}, k_{ascend} \in [0, 1]$ are constant parameters determining the downscale factor of positive and negative ice surface slopes, respectively, and

$$\text{sat}^+(s) = \begin{cases} x, & \text{if } x > 0 \\ 0, & \text{otherwise,} \end{cases} \quad \text{sat}^-(s) = \begin{cases} x, & \text{if } x < 0 \\ 0, & \text{otherwise.} \end{cases}$$

are saturation functions only letting through positive and negative numbers, respectively. The motivation for using two different downscale parameters, is that one may wish that the vehicle is more sensitive to positive slopes as they increase the probability of collision, i.e. choose the factors such that $k_{dive} \geq k_{ascend}$.

The proposed altitude guidance law is given by

$$\begin{aligned} \theta_d :&= -\text{arctan}\left(\frac{\hat{a} - a_d + \varpi_s \Delta_z}{\Delta_z}\right) \\ &= -\text{arctan}\left(\frac{\hat{a} - a_d}{\Delta_z} + \varpi_s\right) \end{aligned} \tag{13}$$

where θ_d is the desired pitch, $\Delta_z > 0$ is a lookahead distance ahead of the vehicle, and $\varpi_s \Delta_z$ is the first-order prediction of the change in the ice surface depth along Δ_z. The desired pitch θ_d is then sent as input to a reference model and then to a pitch controller. The general idea of the altitude LOS guidance law is shown in Figure 1.

The steering law in (13) may be interpreted as a saturating proportional feedback controller with a feedforward term:

$$\theta_d = -\text{arctan}\left(k_p(a - a_d) + v_{ff}\right) \tag{14}$$

where $k_p = 1/\Delta_z$ is the proportional gain, and $v_{ff} = \varpi_s$ is the feedforward term. The feedforward term will ensure that the vehicle responds instantly to changes in the ice surface slope.

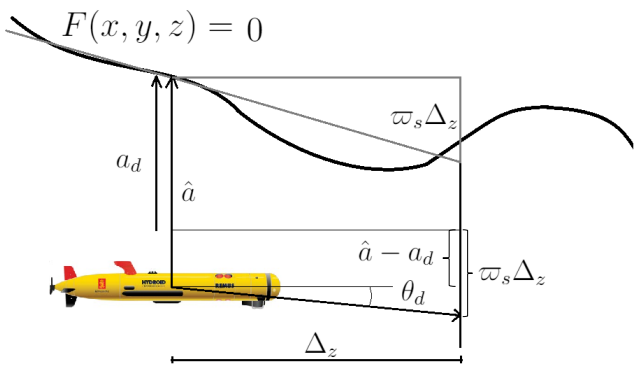

Fig. 1. Altitude LOS guidance law with $k_{dive} = k_{ascent} = 1.0$.

IV. Development of Bayesian risk model

This section presents the development of the Bayesian network risk model for online reasoning over the current state of risk. This will later be used for autonomous risk-based decision-making.

Thieme and Utne [8] follow a well-structured five steps process to develop Bayesian networks for autonomous systems:

1) Describe aim and context of the Bayesian network.
2) Gather and group information relevant for the context into nodes.
3) Connect the nodes with directional arcs.
4) Determine the conditional probability tables and quantify the model.
5) Test and validate the model.

This process has been adapted in this paper for developing the Bayesian network.

A. Aim and context of Bayesian network

In this case study, the AUV operates under the sea ice with the objective of following a contour of the ice surface (under-ice altitude control). We assume that the AUV operates in an area with pre-installed subsea acoustic positioning system infrastructure consisting of transducers, which it uses to determine its reference positions in a reliable manner. The navigational uncertainty from the acoustic positioning system is assumed to be dependent on the distance between the AUV and the transducers. The AUV uses an upwards-looking DVL to estimate its altitude relative to the ice surface.

We want to reason over the current state of the risk during the mission, or more specifically, the risk of losing the vehicle. The decision problem is to autonomously select and reselect the altitude setpoint, given its belief about the current state of risk.

By gathering in-situ sensor data, the posterior distribution of the risk state is updated online. The posterior probability distribution of the risk state should provide some information about the probability of something going wrong, and the consequences of that happening. Figure 2 shows a generic Bayesian network structure following this idea.

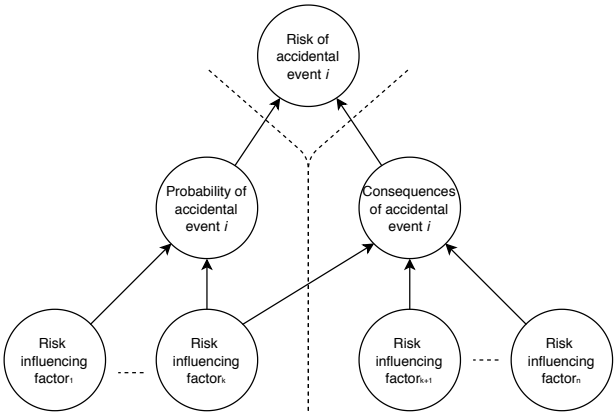

Fig. 2. Generic structure of Bayesian network for calculating the risk of a hazardous event. A series of these trees may be connected to a new root node when including multiple hazardous events. Note that one risk influencing factor may influence both the probability and the consequence(s) of an accidental event.

B. Grouping of relevant information

The risk of losing the vehicle is captured in the Bayesian network by the target node *risk state*. The risk state is influenced by the probability of losing the vehicle and the consequences of losing the vehicle, captured by the two intermediate nodes *susceptibility* and *recovery ineffectiveness*, respectively.

In Huang et al. [13], the Performance Measures Framework for Unmanned Systems (PerMFUS) is proposed, which is a multiple-axis performance metrics model for unmanned systems. This framework characterizes the system performance requirements by: i) the mission that are to be carried out, ii) the environment in which the missions are to be performed, and iii) the characteristics of the system itself. In this paper, we adopt this framework in order to further group the relevant information for the susceptibility of the vehicle. This is captured by the three intermediate nodes *system degradation*, *environmental complexity* and *mission complexity*, which are the parents of the susceptibility node.

Further, we group information that is measurable or directly observable, e.g. from algorithms processing sensor data, into observable nodes. These variables will be the leaf nodes of the network.

For simplicity, all variables in the Bayesian network are given three discrete states, 0, 1 and 2, representing low, medium and high severity, respectively. In order to be stringent, note that all nodes have been defined with negative attributes.

C. Connecting the nodes with directional arcs

We now provide a structural description of the proposed Bayesian network. For simplicity, we have decided to restrict each intermediate node with two observable parent nodes each.

1) System degradation: After discussions with experts on AUVs, particularly two observable variables are thought to

influence the integrity of the system itself, namely the navigational uncertainty and the remaining power capacity. These have been added as parent nodes of the system degradation node.

2) Environmental complexity: According to Brito and Griffiths [4] objects, seabed slope, underwater hazards, metocean conditions, ice concentration and ice thickness can affect the probability of vehicle loss in open sea, around coastal waters and under ice covers. The gradient of the ice surface may, in addition to give information about the ice surface slope, give an indication of the presence of unstructured ice and obstacles. Also, the ocean current velocity is thought to be the most important metocean condition. Therefore, the ice surface gradient and ocean current velocity have been chosen as the observable nodes influencing the environmental complexity.

3) Mission complexity: Many factors may influence the mission complexity. In this model, we have added what we believe are the two most important factors: the total path length, and the setpoint for the altitude controller, which maintains a desired distance to the ice.

4) Recovery ineffectiveness: Recovery ineffectiveness says something about the severity of vehicle loss, i.e. how difficult it will be to recover the vehicle again. Ice thickness will influence the recovery ineffectiveness, as a hole must typically be drilled in the ice in order to recover the vehicle. Intuitively, the severity of vehicle loss will also increase with the distance to the base. These two variables have been added as observable parent nodes.

Figure 3 shows the proposed Bayesian network online risk model.

D. Quantification of conditional probability distributions

Quantifying the CPTs of the variables is a difficult task. It is possible to learn the causalities from data, but often, the amount of data is too scarce for such approaches. Therefore, expert elicitation is the preferred approach in this case.

The process of CPT assessment was adapted from [8], where either a high or low strength of influence from a parent node to a child node is given in order to calculate the CPT. The strength of influence defines the spread in the template for a given parent state. Table I shows the CPT templates for assessment of the child nodes.

Parent's state	Child's states	Low strength template	High strength template
Worst	Worst	0.60	0.90
	Intermediate	0.30	0.09
	Best	0.10	0.01
Intermediate	Worst	0.20	0.05
	Intermediate	0.60	0.90
	Best	0.20	0.05
Best	Worst	0.10	0.01
	Intermediate	0.30	0.09
	Best	0.60	0.90

TABLE I

DISCRETIZED CPT TEMPLATES FOR LOW AND HIGH STRENGTH OF INFLUENCE. WORST, INTERMEDIATE AND BEST REPRESENT THE STATES GENERICALLY.

All arcs from the child nodes to its parent nodes are assessed with a low or high strength of influence. The strength of influence will then determine the weight of each arc: a weight of 1 and 3 are associated with a low strength of influence and a high strength of influence, respectively. The resulting weights are then normalized with the total sum of all weights. A child node's CPT is then calculated by multiplying the template of all arcs with their respective normalized weights, for all combinations of the parent nodes' and child node's states.

In Table II, the assigned strength of influence of each node is shown.

Parent name	Child name	Influence strength
Navigational uncertainty	System degradation	High
Power capacity	System degradation	Low
Ice surface gradient	Environmental complexity	High
Ocean current velocity	Environmental complexity	High
Desired altitude	Mission complexity	High
Total path length	Mission complexity	Low
System degradation	Susceptibility	High
Environmental complexity	Susceptibility	High
Mission complexity	Susceptibility	High
Ice thickness	Recovery ineffectiveness	High
Distance to base	Recovery ineffectiveness	High
Susceptibility	Risk state	High
Recovery ineffectiveness	Risk state	Low

TABLE II

CAUSAL STRUCTURE OF BAYESIAN NETWORK AND THE ASSIGNED STRENGTHS OF INFLUENCE.

V. RISK-BASED DECISION-MAKING

In this section, we extend the Bayesian network risk model to a decision network for autonomous risk-based selection and reselection of the altitude setpoint.

A. Risk index

In the decision network, we want to represent the risk with a real number rather than a probability distribution over discrete states. We define the risk index $ri \in [0, 1]$ as the estimated value of the risk state, ranging from low risk at 0 to high risk at 1. This is captured by a utility node in the decision network. Figure 4 shows the relation between the value of the risk index and the discrete risk states. The risk index ri is calculated from the discrete probability distribution of the risk state according to

$$\begin{aligned} ri &= E(Risk|a_s, parents(Risk)) \\ &= \sum_{i=1}^{n} P[Risk = risk_i|a_s, parents(Risk)]f(risk_i) \end{aligned} \tag{15}$$

where $parents(Risk)$ denotes the values of the parents of the risk state variable, $E(Risk|a_s, parents(Risk))$ is the expected posterior risk state given the altitude setpoint and its parents, and $f : \{0, 1, 2\} \longrightarrow \{0, 0.5, 1\}$ is a discrete function that maps a risk state to its corresponding value.

Figure 5 shows the risk index for the worst case, medium case and best case - that is, all observable nodes have been assigned the worst, medium or best state as evidence, respectively, as a function of the altitude setpoint.

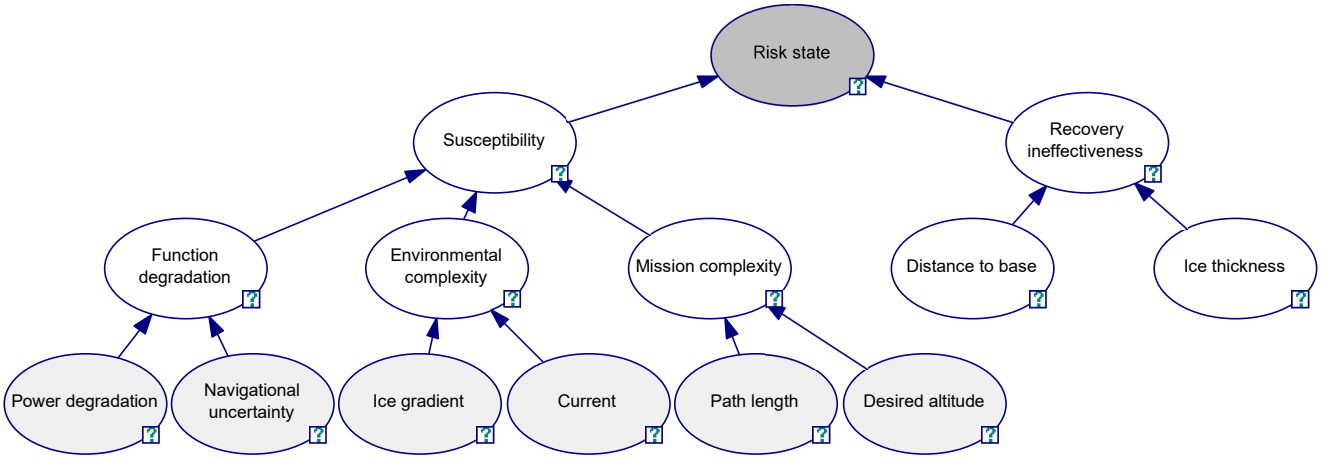

Fig. 3. Bayesian network for online calculation of risk during an under-ice operation of AUVs. Node color-coding: light grey, observable nodes; white, intermediate nodes; dark grey, target nodes.

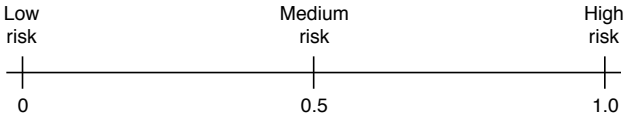

Fig. 4. The risk index. The discrete risk states low, medium and high correspond to the numerical values 0.0, 0.5 and 1.0, respectively.

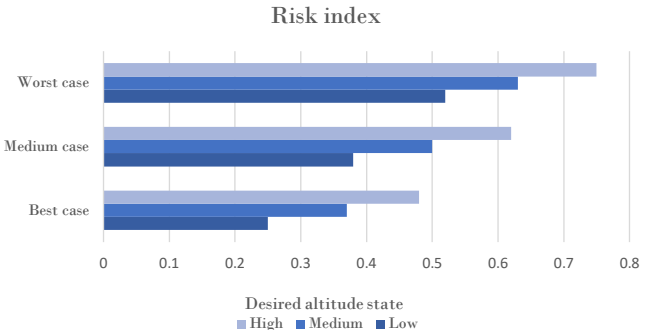

Fig. 5. The risk index as a function of the desired altitude state for the worst, medium and best case.

B. Online reasoning

Online reasoning refers to the continuous update of the network as new evidence are obtained. At every time step, sensor data for the observable nodes are discretized into states 0, 1 and 2, representing low, medium and high severity, and updated as evidence accordingly. The posterior probability distribution of the risk state and the risk index are calculated thereafter.

A dwell-time is implemented in the update of variables in the network. When an evidence that increases the severity of a variable is obtained from the sensor data, the network is updated immediately. This evidence will then be fixed for a given amount of time t_{min}, before the same variable is allowed be updated with new evidence that reduces the risk, unless the new evidence has an even higher severity. Thus, we get a conservative approach to updating the risk belief: the AUV will update its beliefs about the current state of risk immediately to possible threats, and this belief will persist for some time, even though the evidence indicates that the threat has seized to exist.

The update rule can be mathematically formulated as

$$ev(k+1) = \begin{cases} ev_{new}, & \text{if } t \geq t_{min} \vee ev_{new} > ev(k) \\ ev(k), & \text{otherwise} \end{cases} \tag{16}$$

where $ev(k)$ is the assigned evidence in the network at time step k, ev_{new} is the most recent obtained evidence, t is the elapsed time since last update, and t_{min} is the dwell-time. Here it is assumed that more severe states have larger values.

C. Decision-making

We want the AUV to autonomously select and reselect the altitude setpoint given its belief about the current state of risk. We therefore replace the observable chance node for the altitude setpoint in the Bayesian network with an action node.

A greedy risk-based decision-making algorithm is proposed. The algorithm greedily chooses the altitude setpoint a_s yielding the highest reward, while the predicted risk index from selecting a_s is constrained by a risk-bound. This may be formulated as

$$a_s^* = \underset{a_s}{\operatorname{argmax}}\, R(a_s) \quad \text{s.t.} \quad ri \leq \delta \tag{17}$$

where a_s^* is the optimal altitude setpoint, $R(a_s)$ is a reward function and δ is a risk-bound which specifies the allowable risk index.

The algorithm will evaluate the decision network for all altitude setpoints, and choose the setpoint yielding the largest reward constrained by the risk-bound. If no setpoint satisfies the risk-bound, a signal to abort the mission will be initiated. Figure 3 shows the proposed risk-based decision network.

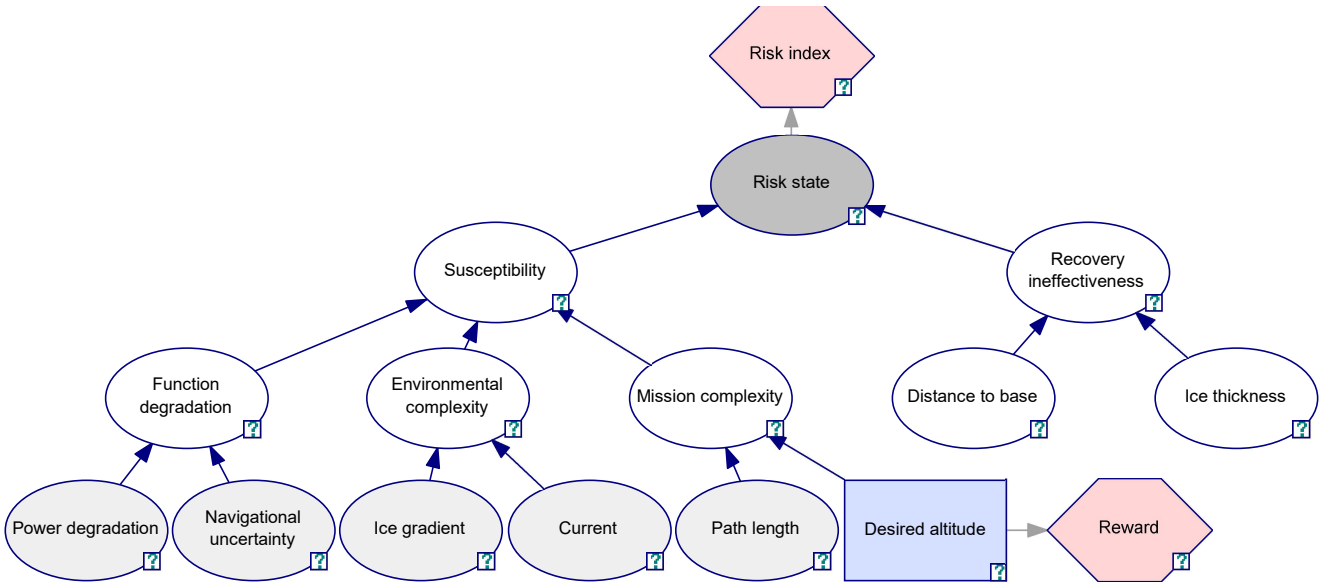

Fig. 6. Decision network for online calculation of risk during an under-ice operation of AUVs. Node color-coding: light grey, observable chance nodes; white, intermediate chance nodes; dark grey, target chance nodes; action nodes, light blue; utility nodes, light red. The objective of the risk-based decision network is to maximize the reward while subject to a constraint on the risk index.

VI. Simulation results and discussion

A. Simulation setup

The simulator environment used in this paper is an Arctic AUV simulator created by Norgren [14] in MATLAB/Simulink and C++. The vehicle dynamics implemented in the simulator is based on the REMUS 100 AUV. The simulated ice data is a three-dimensional floe-scale map of a sea-ice draft compiled from expeditions by an AUV to the near-coastal regions of the Weddell, Bellingshausen, and Wilkes Land sectors of Antarctica, developed by Williams et al. [15] and [16]. The Bayesian network was implemented in Simulink with C++ using the `dlib` package [17].

B. Case studies

In this paper, we simulate a mission under ice where the desired motion of the AUV is a zig-zag trajectory in the horizontal plane, composed of a set of linear path segments, while the altitude setpoint is autonomously selected and controlled based on DVL measurements. The implemented set of possible altitude setpoints is $a_s \in A_s = \{-10, -15, -20\}[m]$. The reward is simply $R(a_s) = -1/a_s$, such that lower altitudes give larger rewards. We present two case studies with different risk-bounds. Case study 1 will have a risk-bound $\delta = 0.65$, and case study 2 will have a risk-bound $\delta = 0.55$. An ocean current velocity of $V_c = 0.3$ m/s is present in the simulations.

All observable network variables are first calculated as continuous values, and then discretized into discrete states 0, 1 and 2, representing low, medium and high severity, respectively. Table III shows the discretization of the observable variables from continuous values.

State	0	1	2	
Navigational uncertainty	< 0.25	$0.25 - 0.5$	> 0.5	[-]
Power degradation	< 50	$50 - 75$	> 75	%
Ice surface gradient	< 0.2	$0.2 - 0.4$	> 0.4	[m/s]
Ocean current velocity	< 0.3	$0.3 - 1$	> 1	[m/s]
Desired altitude	-10	-15	-20	[m]
Total path length	< 1	$1 - 3$	> 3	[km]
Ice thickness	< 1.5	$1.5 - 3$	> 3	[m]
Distance to base	< 200	$200 - 500$	> 500	[m]

TABLE III
Discretization of observable nodes in the network.

C. Simulation results

Figure 7-8 show the vertical trajectory, risk index and evidence evolution over time for case study 1. Figure 10-11 show the same results for case study 2. Figure 9 shows the 3D trajectory beneath the ice surface, and Figure 12 shows the corresponding trajectory in the horizontal plane.

As seen in Figure 7 and 10, the risk index is continuously updated and the risk-bound is satisfied in both cases. When obtaining an evidence that makes the risk index exceed the risk-bound, the risk is mitigated by selecting an altitude setpoint further away from the ice surface.

As expected, the AUV spends more time closer to the ice surface in case study 1 with a higher risk-bound δ. The risk-bound should be chosen by the operators based on their risk appetite prior to the mission.

Some collision avoidance properties are obtained from the proposed method: i) due to the feedforward term in (13), the AUV will react instantly to changes in the slope of the ice surface, and ii) an altitude setpoint further away from the ice may be autonomously selected in situations with higher risks. However, some collision avoidance system utilizing forwards-

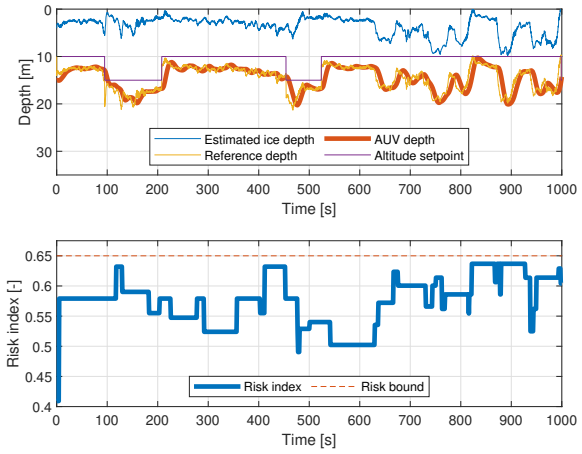

Fig. 7. Vertical trajectory of the AUV and risk index with $\delta = 0.65$.

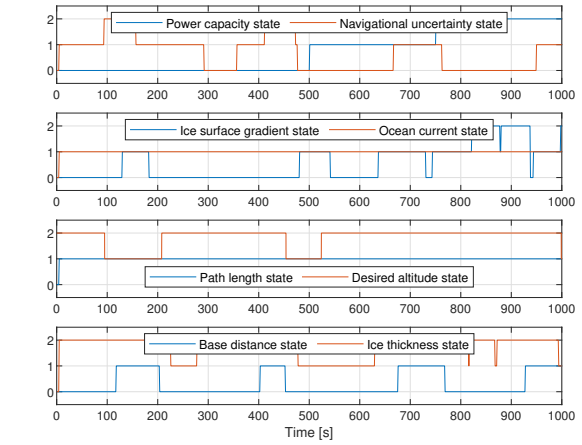

Fig. 8. Evolution of the evidence in the Bayesian network with $\delta = 0.65$.

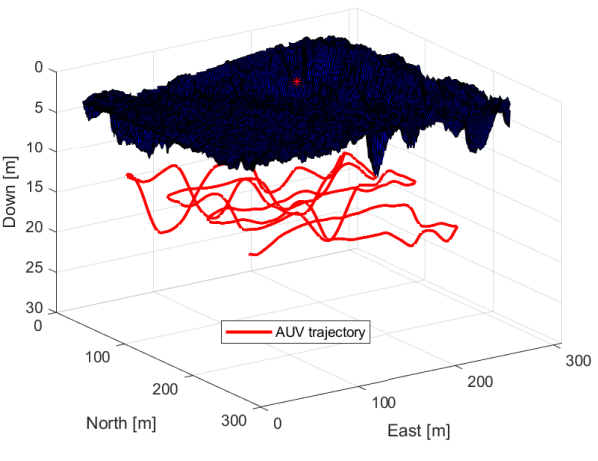

Fig. 9. 3D trajectory of the AUV under the ice surface

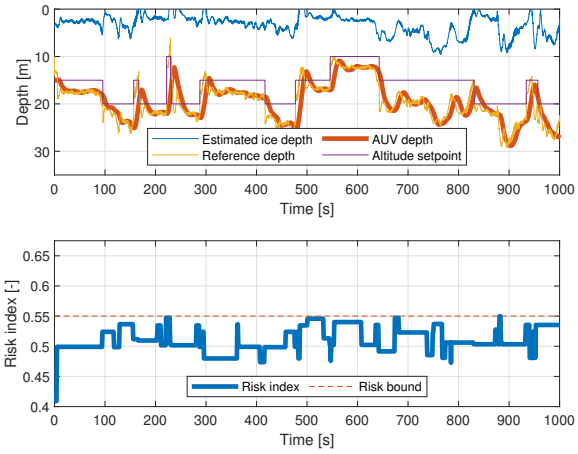

Fig. 10. Vertical trajectory of the AUV and risk index with $\delta = 0.55$.

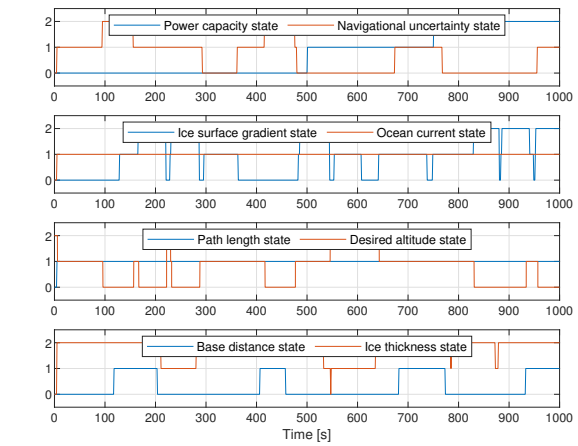

Fig. 11. Evolution of the evidence in the Bayesian network with $\delta = 0.55$.

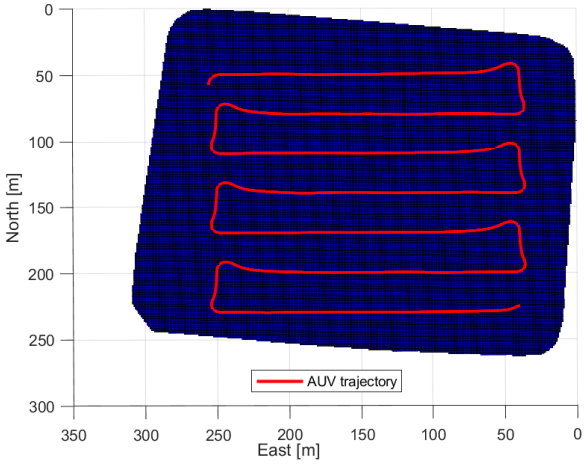

Fig. 12. Trajectory of the AUV in the horizontal plane

looking sonars that overrides the altitude controller is still needed.

For future work, a thorough comparison of the guidance scheme with and without the ice surface slope feedforward should be conducted. A more extensive Bayesian network risk model should be developed. Extending the risk model to a dynamic Bayesian network for modeling the temporal aspect of risk is of interest. This will be useful for autonomous planning, as the predicted future evolution of risk may be taken into account. Also, including a dynamic risk-bound, which may be a function of e.g. the expected reward or uncertainties in the estimates, is suggested for further work.

VII. Conclusion

A method for intelligent risk-based under-ice altitude control is presented. Firstly, an altitude guidance law for following a contour of the ice surface via pitch control using DVL measurements is proposed. A desired pitch angle is computed based on the estimated altitude error and a feedforward on the estimated slope of the ice surface in the vehicle heading direction. Furthermore, a Bayesian network is developed for online reasoning over the risk of vehicle loss, where the probability of vehicle loss is captured in a susceptibility node, and the consequences of vehicle loss is captured in a recovery ineffectiveness node. Evidential reasoning is used to update the posterior probability distribution over the current state of risk from the continuous updates of evidences from sensor data. This model is then extended to a decision network for autonomous selection and reselection of the setpoint for the altitude controller. The AUV will at a given time select the altitude setpoint yielding the largest reward while subject to a constraint on the risk. The risk-bound is tuned according to the operators' appetite for risk. Simulations show that the AUV successfully adapts to the varying level of risk throughout its mission by reselecting the altitude setpoint.

References

[1] J. Strutt, "Report of the inquiry into the loss of autosub2 under the fimbulisen," Project Report, 2006, deposited at the request of Prof. Gwyn Griffiths on behalf of Autosub team. [Online]. Available: https://eprints.soton.ac.uk/41098/

[2] M. Rausand, *Risk Assessment: Theory, Methods, and Applications*, ser. Statistics in practice. John Wiley Sons Inc, 2013.

[3] I. B. Utne, A. J. Sørensen, and I. Schjølberg, "Risk management of autonomous marine systems and operations," 06 2017, p. V03BT02A020.

[4] M. Brito and G. Griffiths, "A bayesian approach for predicting risk of autonomous underwater vehicle loss during their missions," *Reliability Engineering and System Safety*, vol. 146, no. C, pp. 55–67, 2016.

[5] G. Griffiths and M. Brito, "Predicting risk in missions under sea ice with autonomous underwater vehicles," in *2008 IEEE/OES Autonomous Underwater Vehicles*. IEEE, 2008, pp. 1–7.

[6] T. Aven, "Practical implications of the new risk perspectives," *Reliability Engineering and System Safety*, vol. 115, pp. 136–145, 2013.

[7] K. B. Korb and A. E. Nicholson, "Bayesian artificial intelligence," *Artificial Intelligence and Law*, vol. 11, no. 4, pp. 289–298, 2003.

[8] C. A. Thieme and I. B. Utne, "A risk model for autonomous marine systems and operation focusing on humanautonomy collaboration," *Proceedings of the Institution of Mechanical Engineers, Part O: Journal of Risk and Reliability*, vol. 231, no. 4, pp. 446–464, 2017.

[9] J. Hegde, I. B. Utne, I. Schjølberg, and B. Thorkildsen, "A bayesian approach to risk modeling of autonomous subsea intervention operations," *Reliability Engineering System Safety*, vol. 175, 2018. [Online]. Available: http://search.proquest.com/docview/2073130157/

[10] S. Russell, "Artificial intelligence : a modern approach," Boston, 2016.

[11] T. I. Fossen, *Handbook of Marine Craft Hydrodynamics and Motion Control*. Chichester, UK: John Wiley Sons, Ltd, 2011.

[12] F. Dukan and A. J. Sørensen, "Sea floor geometry approximation and altitude control of rovs," *Control Engineering Practice*, vol. 29, pp. 135–146, 2014.

[13] H.-M. Huang, E. Messina, and A. Jacoff, "Performance measures framework for unmanned systems (permfus): initial perspective," in *Proceedings of the 9th Workshop on performance metrics for intelligent systems*, ser. PerMIS '09. ACM, 2009, pp. 65–72.

[14] P. Norgren, "Autonomous underwater vehicles in arctic marine operations : Arctic marine research and ice monitoring," Trondheim, 2018.

[15] G. Williams, T. Maksym, J. Wilkinson, C. Kunz, C. Murphy, P. Kimball, and H. Singh, "Thick and deformed antarctic sea ice mapped with autonomous underwater vehicles," *Nature Geoscience*, vol. 8, no. 1, pp. 61–67, 2015. [Online]. Available: http://search.proquest.com/docview/1657287407/?pq-origsite=primo

[16] G. D. Williams, T. Maksym, C. Kunz, P. Kimball, H. Singh, J. Wilkinson, T. LachlanCope, E. Trujillo, A. Steer, R. Massom, K. Meiners, P. Heil, J. Lieser, K. Leonard, and C. Murphy, "Beyond point measurements: Sea ice floes characterized in 3d," *Eos, Transactions American Geophysical Union*, vol. 94, no. 7, pp. 69–70, 2013.

[17] D. E. King, "Dlib-ml: A machine learning toolkit," *Journal of Machine Learning Research*, vol. 10, pp. 1755–1758, 2009.

REMUS AUV model

The values for the 6 DOF equation of motion (18) implemented in the simulator are taken from [24]. The ridid-body, added mass and damping matrices for the REMUS 100 AUV are as follows:

$$\boldsymbol{C}_{RB} = \begin{bmatrix} 30.479 & 0 & 0 & 0 & 0.597 & 0 \\ 0 & 30.479 & 0 & -0.597 & 0 & 0 \\ 0 & 0 & 30.479 & 0 & 0 & 0 \\ 0 & -0.597 & 0 & 0.189 & 0 & 0 \\ 0.597 & 0 & 0 & 0 & 3.462 & 0 \\ 0 & 0 & 0 & 0 & 0 & 3.45 \end{bmatrix} \tag{63}$$

$$\boldsymbol{M}_A = \begin{bmatrix} 0.93 & 0 & 0 & 0 & 0 & 0 \\ 0 & 35.5 & 0 & 0 & 0 & -1.93 \\ 0 & 0 & 35.5 & 0 & 1.93 & 0 \\ 0 & 0 & 0 & 0.07 & 0 & 0 \\ 0 & 0 & 1.93 & 0 & 4.88 & 0 \\ 0 & -1.93 & 0 & 0 & 0 & 4.88 \end{bmatrix} \tag{64}$$

$$\boldsymbol{D}(\boldsymbol{\nu}_r) = \begin{bmatrix} 1.62|u_r| & 0 & 0 & 0 & 0 & 0 \\ 0 & 1310|v_r| & 0 & 0 & 0 & -0.632|r| \\ 0 & 0 & 1310|w_r| & 0 & 0.632|q| & 0 \\ 0 & 0 & 0 & 0.13|p| & 0 & 0 \\ 0 & 0 & -3.18|w_r| & 0 & 188|q| & 0 \\ 0 & 3.18|v_r| & 0 & 0 & 0 & 188|r| \end{bmatrix} \tag{65}$$

The rigid-body and added mass centripetal and Coriolis matrices, denoted as $\boldsymbol{C}(\boldsymbol{\nu}_r) = \boldsymbol{C}_{RB}(\boldsymbol{\nu}) + \boldsymbol{C}_A(\boldsymbol{\nu}_r)$ are given by:

$$\boldsymbol{C}_{RB} = \begin{bmatrix} \boldsymbol{0}_{3\times 3} & -m\boldsymbol{S}(\boldsymbol{v}^b_{auv}) - m\boldsymbol{S}(\boldsymbol{\omega}^b_{auv})S(\boldsymbol{r}^b_g) \\ -m\boldsymbol{S}(\boldsymbol{v}^b_{auv}) + m\boldsymbol{S}(\boldsymbol{r}^b_g)S(\boldsymbol{\omega}^b_{auv}) & -\boldsymbol{S}(\boldsymbol{I}_b\boldsymbol{\omega}^b_{auv}) \end{bmatrix} \tag{66}$$

$$\boldsymbol{C}_A = \begin{bmatrix} \boldsymbol{0}_{3\times 3} & -\boldsymbol{S}(\boldsymbol{A}_{11}v^2_{auv} + \boldsymbol{A}_{12}\omega^2_{auv}) \\ -\boldsymbol{S}(_{11}v^2_{auv} + \boldsymbol{A}_{12}\omega^2_{auv}) & -\boldsymbol{S}(\boldsymbol{A}_{21}v^2_{auv} + \boldsymbol{A}_{22}\omega^2_{auv}) \end{bmatrix} \tag{67}$$

where $\boldsymbol{S}(\boldsymbol{r}^b_g) = -\boldsymbol{S}^T(\boldsymbol{r}^b_g) \in \mathbb{R}^{3\times 3}$ is a skew-symmetric matrix, $\boldsymbol{r}^b_g$ represents the location of the AUV's center of gravity with respect fo the CO, I_b represents the inertia tensor and $\boldsymbol{A}_{ij} \in \mathrm{R}^{3\times 3}$ given by

$$\boldsymbol{M}_A = \begin{bmatrix} \boldsymbol{A}_{11} & \boldsymbol{A}_{12} \\ \boldsymbol{A}_{21} & \boldsymbol{A}_{22} \end{bmatrix} \tag{68}$$

The propeller coefficients are taken from [41]. The remaining parameters for the REMUS 100 AUV are given by Table 2.

Table 2: REMUS 100 AUV parameters

Description	**Symbol**	**Value**
CG lever arm w.r.t. CO	r_g^b	$[0, 0, 0.0196]$ $[m]$
CB lever arm w.r.t. CO	r_b^b	$[0, 0, 0]$ $[m]$
Weight of vehicle	W	$299[N]$
Vehicle buoyany	B	$306[N]$
Density of sea water	ρ	$1025[kg/m^3]$
Fin lift coefficient	$c_{L,\alpha}$	$3.12[-]$
Fin surface area	S_{fin}	$6.65 \times 10^{-3}[m^2]$
Fin placement w.r.t. CO	x_{fin}	$-0.638[m]$
Thrust coefficient	K_T	$2.5075[-]$
Torque coefficient	K_Q	$0.3203[-]$
Propeller diameter	D_{prop}	$0.1397[m]$